EUROPEAN COMMISSION

Community research

GOBIERNO DE ESPAÑA MINISTERIO DE ECONOMÍA Y COMPETITIVIDAD

Ciemat Centro de Investigaciones Energéticas, Medioambientales y Tecnológicas

PEBS Long-term Performance of Engineered Barrier Systems

**Long-term Performance of Engineered Barrier Systems PEBS**

# Long-term THM tests reports: THM cells for the HE-E test: setup and first results

## (DELIVERABLE-N°: D2.2-7.1)

**Contract (grant agreement) number: FP7 249681**

CIEMAT Technical Report CIEMAT/DMA/2G210/03/2012

Author(s):
M.V. Villar, P.L. Martín, R. Gómez-Espina, F.J. Romero, J.M. Barcala

Reporting period:
Date of issue of this report: June 30th 2012

**Project co-funded by the European Commission under the Seventh Euratom Framework Programme for Nuclear Research &Training Activities (2007-2011)**

Start date of project: 01/03/10 Duration : 48 Months

| Dissemination Level | | |
|---|---|---|
| **PU** | Public | **PU** |
| **RE** | Restricted to a group specified by the partners of the [acronym] project | |
| **CO** | Confidential, only for partners of the [acronym] project | |



EURATOM

# Contents



# Acknowledgements

The research leading to these results has received funding from the European Atomic Energy Community's Seventh Framework Programme (FP7/2007-2011) under Grant Agreement n°249681, the PEBS project. This work is being additionally financed by ENRESA through a CIEMAT-ENRESA General Agreement.

# 1 Introduction

A common design of a high-level radioactive waste (HLW) disposal system consists of the wastes encapsulated within steel canisters that are emplaced within horizontal tunnels, with the space between the canisters and the surrounding rock filled with a bentonite-based material. In the early post closure period the buffer is expected to experience the maximum temperature. In this phase the buffer is largely unsaturated and the thermal evolution of the EBS is likely to be controlled by the effective thermal conductivity of dry buffer.

In particular, the temperature evolution of the engineered barrier system and surrounding rock was simulated using reference data for the thermal properties of HLW, bentonite backfill and Opalinus Clay. The results showed that the surface temperatures would reach a maximum value of ~150°C within a few years after emplacement (Johnson *et al*. 2002). These anticipated temperatures at the canister surface, in the bentonite and at the bentonite-host rock interface were scaled down in time and space to meet the specifications of the HE-E experiment, which is being carried out in the framework of PEBS (Gaus *et al*. 2011). The HE-E experiment targets the period immediately after repository closure when the temperatures are maximal and the moisture content is low but increasing.

The HE-E experiment is a 1:2 scale heating experiment considering natural resaturation of the EBS and a maximum heater surface temperature of 140°C. Heater temperature is foreseen to increase almost linearly to its maximum value in a period of 1 year after which the temperature will be held constant for the years to follow. The experiment is located at the Mont Terri URL (Switzerland) in a 50-m long non-lined horizontal microtunnel of 1.3 m diameter excavated in 1999 in the shaly facies of the Opalinus Clay. The test section of the microtunnel was characterised in detail during the Ventilation Experiment (ENRESA 2005). The detailed design of the experiment is described in Teodori & Gaus (2011).

The experiment consists of two independently heated sections (Figure 1), where the heaters are placed in a steel liner supported by MX80 bentonite blocks (dry density 1.81 g/cm$^3$, water content 10.3%). The two sections are fully symmetric apart from the granular filling material: whereas section one is filled with pure MX80 bentonite pellets, section 2 is filled with a 65/35 granular sand/bentonite mixture with the characteristics described below:

- granular bentonite (B) and bentonite blocks are used in one section of the test, corresponding to the Swiss disposal concept. It is the same as the one used for the ESDRED project, mixture type E (sodium bentonite MX-80 from Wyoming). The material is described in detail in Plötze & Weber (2007). Once emplaced its water content was 5.9% and the dry average density was 1.46 kg/m$^3$.
- sand/bentonite (S/B) mixture (having a higher thermal conductivity) and bentonite blocks are used in the other section. The sand/bentonite mixture was provided by MPC (Limay, France). The components are 65 % of quartz sand with a grain spectrum of 0.5 – 1.8 mm and 35 % of sodium bentonite GELCLAY WH2 (granular material of the same composition as MX-80) of the same grain spectrum, which was obtained by crushing and sieving from the qualified raw material. Water content was 13 % for the bentonite and 0.05 % for the sand, giving a total water content of the mixture in the range of 4%. There is some uncertainty about the actual emplaced density of the mixture, and values as low as 1.26 g/cm$^3$ have been given. However, based on the tests performed to check the emplacement technique, a value of 1.5 g/cm$^3$ has been taken for the calculations and the laboratory tests.

A heater system, capable of representing the temperature curve of the anticipated heat production in the canisters (up to a maximum of 140°C), was switched on the 28th June 2011. During the experiment the temperature, humidity and the water saturation are monitored through a system of sensors on the heater surface within the liner, in the bentonite and in the surrounding host rock.

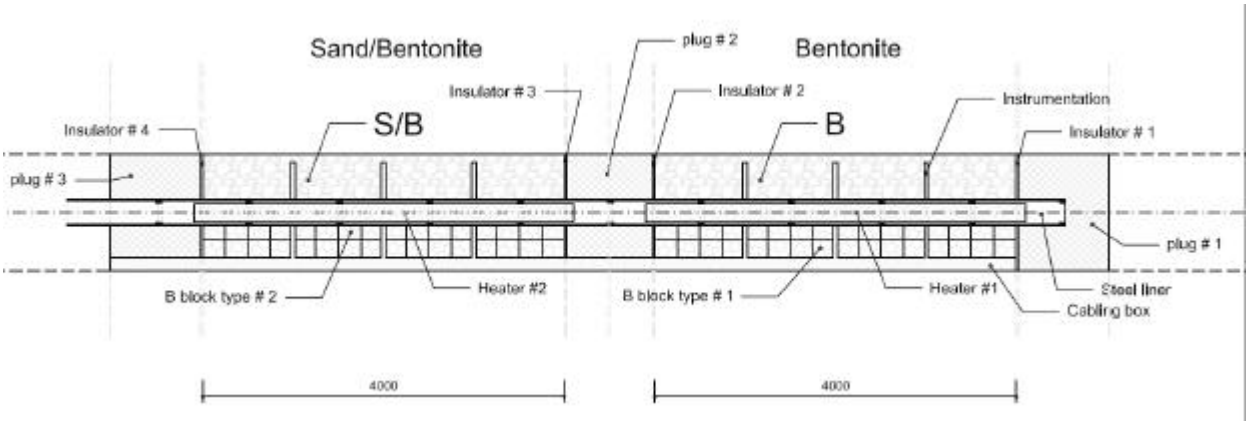


**Figure 1: Layout of the *in situ* HE-E experiment**

The performance of tests at different scales, in both the laboratory and the field, is very useful to observe the thermo-hydro-mechanical processes taking place in the engineered barriers and the geological medium. They also provide the information required for the verification and validation of mathematical models of the coupled processes and their numerical implementation. The laboratory tests in cells are particularly helpful to identify and quantify processes in a shorter period of time and with less uncertainty regarding the boundary conditions than the *in situ* tests. In the tests in cells the sealing material is subjected simultaneously to heating and hydration in opposite directions, in order to simulate the conditions of the clay barrier in the repository. With the aim of complementing the information provided by the HE-E *in situ* test, CIEMAT has undertaken, in the framework of the PEBS project, the performance of two tests in cells simulating the conditions of the sealing materials used in the two sections of the *in situ* test. The description of the experimental setups and materials used as well as the first results obtained are given in this report.

# 2 Material

The materials used in the cells are the same as those used in the *in situ* test and were sent to CIEMAT directly from the Mont Terri test site. A plastic bucket with 25 kg of the sand/bentonite mixture (S/B) was received at CIEMAT on April 2011 and 20 kg of the bentonite pellets (B) were received on June 2011 (Figure 2). The as-received water content of the materials was 6.4% for the pellets and 3.6% for the sand/bentonite mixture. The granulometric curve of both materials obtained by dry sieving is shown in Figure 3. It was checked that the granulometric curve of the bentonite granulate received at CIEMAT coincide with the granulometric curves of the material used for the ESDRED experiment (Figure 4).

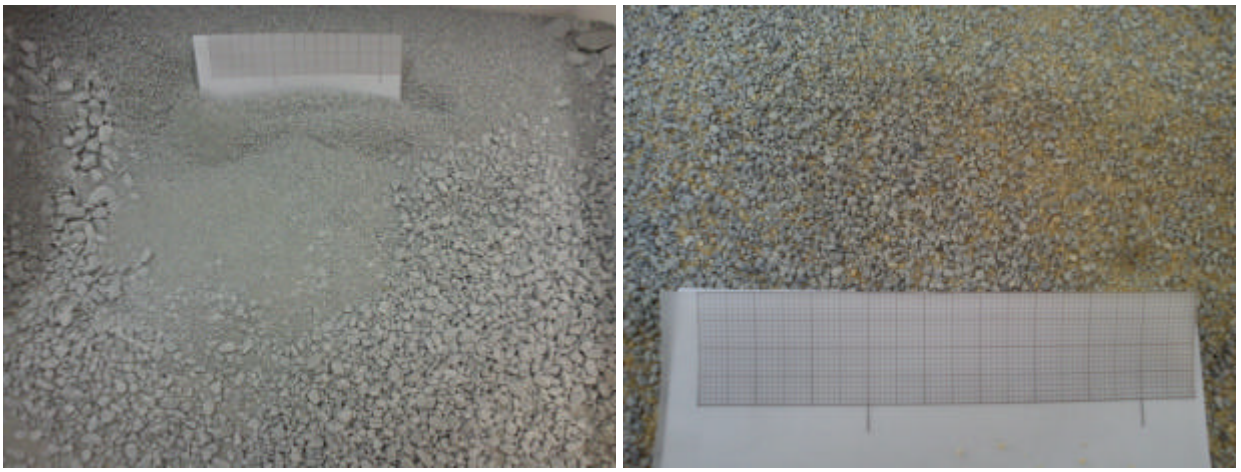

**Figure 2: Appearance of the materials received at CIEMAT: MX-80 pellets (left) and sand/bentonite mixture (right)**

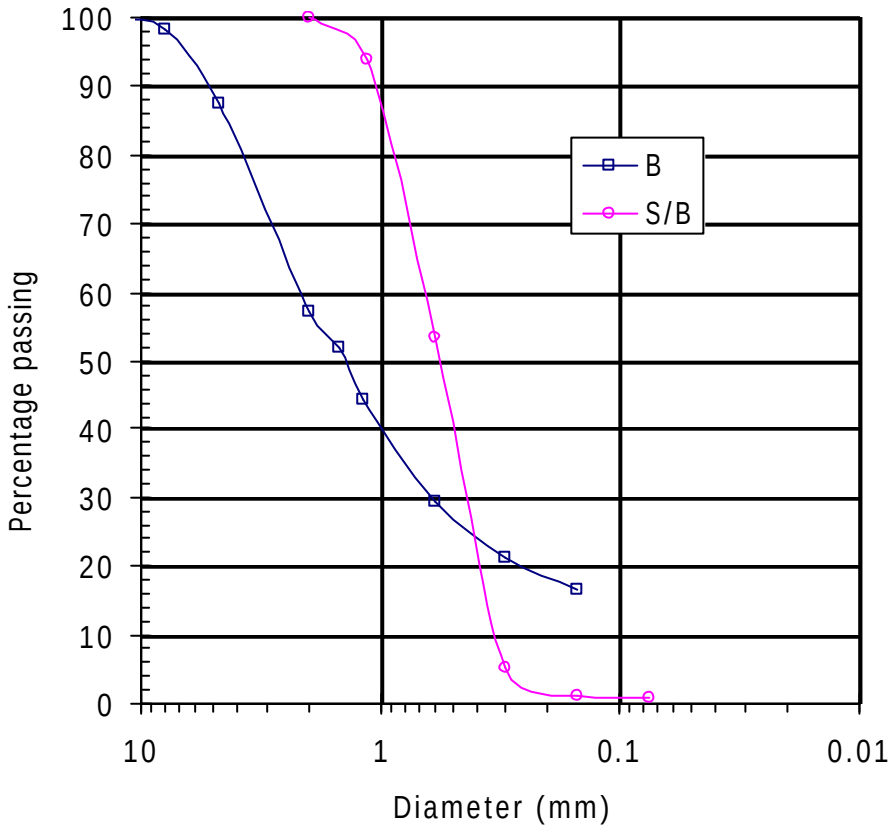


**Figure 3: Granulometric curve obtained by dry sieving of the two materials used in the tests (B: bentonite pellets, S/B: sand/bentonite mixture)**

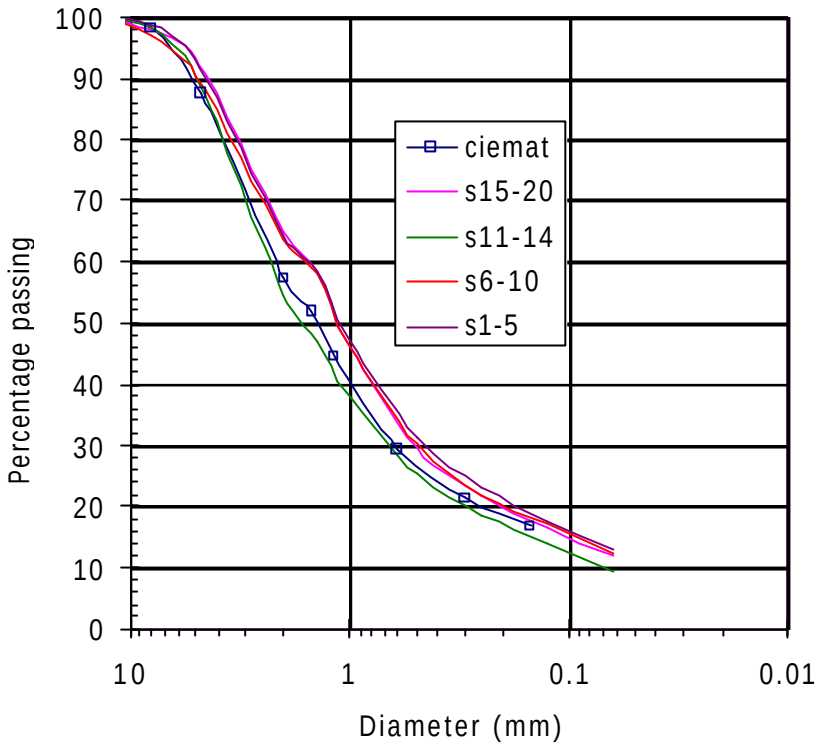


**Figure 4: Comparison of the granulometric curve obtained at CIEMAT for the bentonite granulate and those obtained by NAGRA in material of the ESDRED test**

The dry density of the solid grains determined with pycnometers using water as dispersing agent was 2.71 g/cm$^3$ for the mixture and 2.75 g/cm$^3$ for the granulate. The external specific surface area determined by the 9-point BET method was 5 m$^2$/g for the mixture and 33 m$^2$/g for the pellets. The superficial thermal conductivity of both materials in their as-received state was determined at room temperature using the transient hot wire method. Values of 0.33 and 0.12 W/m·K were obtained for the mixture and the granulate, respectively. The specific heat capacity of both materials ground and dried at 110°C was determined in a TG-DSC Setsys Evolution 16 equipment. The determinations were performed in the range of temperatures from 22 to 298°C. The values obtained for the mixture ranged between 0.74 J/g·K (at 22°C) and 0.90 J/g·K (at 115°C), and for the pellets between 0.64 J/g·K (at 22°C) and 0.97 J/g·K (at 115°C) (Fernández 2011).

The swelling pressure of the sand/bentonite mixture was determined in standard oedometers in samples initially compacted at a nominal dry density of 1.45 g/cm$^3$. Two tests were performed using deionised water to saturate the samples and two others using Pearson water. This solution is sodium rich and has a composition similar to the Opalinus Clay formation pore water. This water has a density of 1.020 g/cm$^3$ (Pearson 1998, Pearson *et al*. 1999). The chemical composition is indicated in Table I. An average swelling pressure of 1.5 MPa was obtained for the samples saturated with deionised water and of 0.7 MPa for the samples saturated with Pearson water.

**Table I: Chemical composition of the water used in the tests (mg/L)**

| $Cl^-$ | $SO_4^{2-}$ | $HCO_3^-$ | $Mg^{2+}$ | $Ca^{2+}$ | $Na^+$ | $K^+$ | $Sr^+$ | pH |
|---|---|---|---|---|---|---|---|---|
| 10635.90 | 1354.41 | 25.75 | 413.19 | 1034.06 | 5550.01 | 62.95 | 44.69 | 7.6 |

# 3 Experimental setup

The infiltration tests are being performed in cylindrical cells similar to cells already used during the FEBEX and NF-PRO projects (Villar *et al*. 2005a, b, 2008). The nominal internal diameter of each cell is 7 cm and inner length 50 cm, therefore, those are the dimensions of the sample columns. The bodies of the cells are made of Teflon to prevent as much as possible lateral heat conduction. The cell with bentonite pellets (called hereafter B) is externally covered with steel semi-cylindrical pieces to avoid the deformation of the Teflon caused by the bentonite swelling. This cover is not necessary in the bentonite/sand mixture cell (call hereafter S/B). Finally, the body of the cells is wrapped with insulation wool to avoid the heat loss.

The material with its hygroscopic water content was poured in seven layers into the cylindrical cells. The bottom part of the cells has a plane stainless steel heater. Inside the upper steel plug of the cells there is a deposit in which water circulates at room temperature (~ 20°C). In this way, a constant gradient between top and bottom of the sample is imposed. Pearson water is injected through the upper lid of the cell. This simulates the water that saturates the barrier in a repository excavated in the Opalinus Clay formation (Mont Terri, Switzerland). A schematic diagram of the setup is shown in Figure 5. The different components of the system are described in detail below.

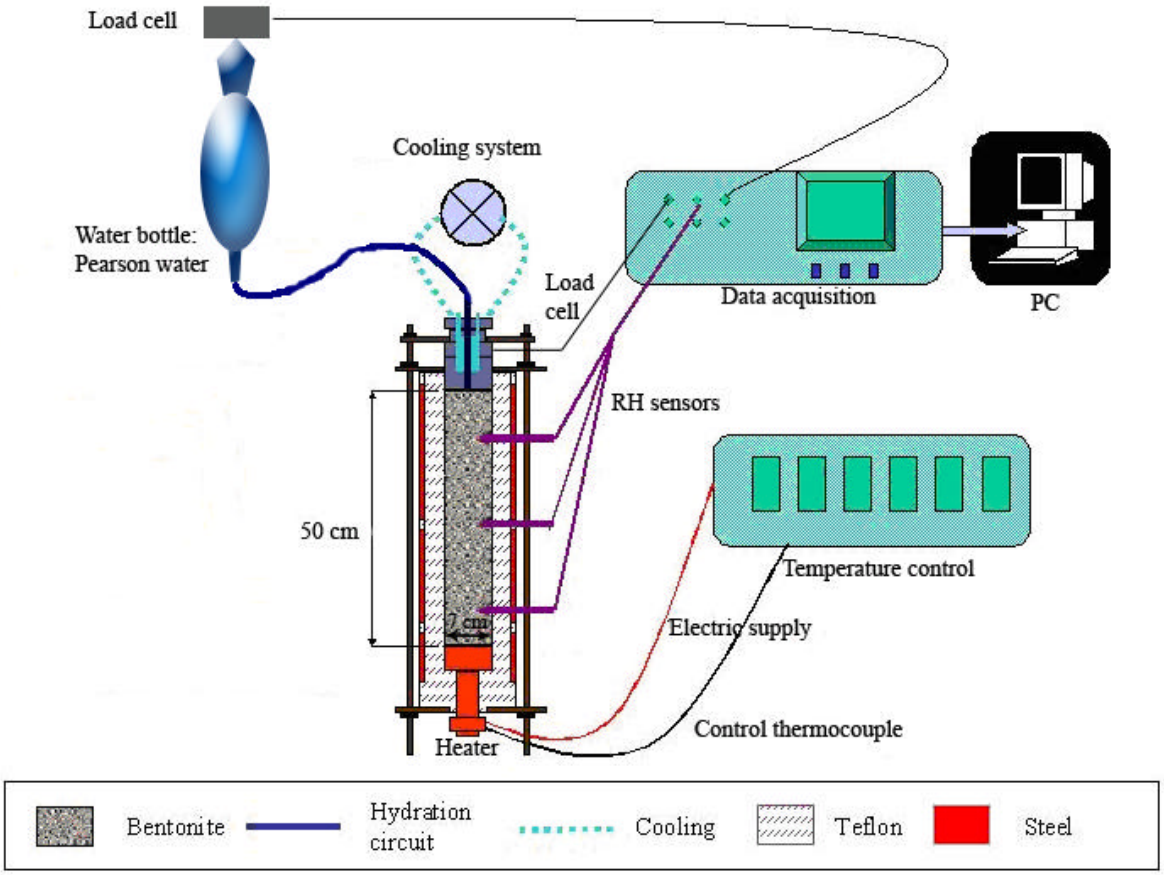


**Figure 5: Experimental setup for the infiltration tests**

## 3.1 DESCRIPTION OF THE CELLS

The body of the cell is constituted by two 200-mm and one 95-mm long cylindrical pieces and a base (Figure 7, item 1). In order to lessen heat dissipation all of them are made of Teflon PTFE, whose thermal conductivity is 0.25 W/m·K. The thickness of the cell wall is 15 mm, and the different pieces are assembled into each other. The watertightness of the contacts between different pieces is guaranteed by means of Viton® o-rings capable of withstanding temperatures of up to 180°C (Figure 7, item 2). The walls of the cells were perforated for the installation of instrumentation (Figure 7, item 4).

In order to reinforce mechanically the wall of cell B, which is to support the swelling pressure of the clay, it has been externally surrounded by semicylindrical pairs of 4-mm thick 304L stainless steel shells (Figure 7, item 3), joint by steel braces. There are 4 pairs of 10-cm long shells and one pair of 5-cm long shells at the bottom, each pair separated from the other by 1.5-cm long Teflon rings (except for the upper pair), in order to break heat transmission along the external steel shells.

The upper closing of the cell is made by means of a 316L stainless steel set, consisting of a plug with lateral o-rings (Figure 7, item 5) to close the cell that includes a chamber for the cooling system (Figure 7, item 6). A central perforation allows the passage of the hydration water through the chamber screwed cap by means of a stainless steel tube, and through the plug by means of a 2 mm diameter perforation (Figure 7, item 7).

The tightening of all the pieces is made by means of six external steel threaded bars (Figure 7, item 8) and plates on top and bottom (Figure 7, item 9). These bars serve as well as support to the cell.

Between the hydration piece and the upper plate, a load cell was located in cell B with the aim of measuring the swelling pressure during the test (Figure 7, item 10). Figure 6 shows the upper section of the cells where the difference in the design of both can be seen: cell B has a load cell and its body is covered with steel pieces, whereas cell S/B does not.

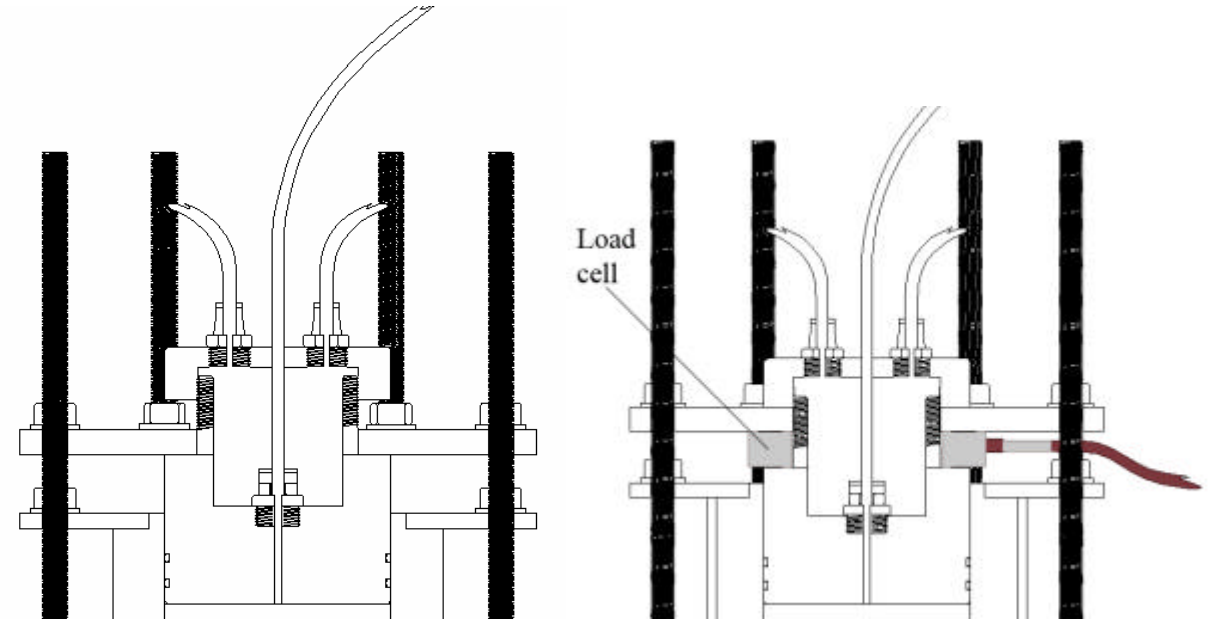


**Figure 6: Upper section of both cells: SB (left) and B (right)**

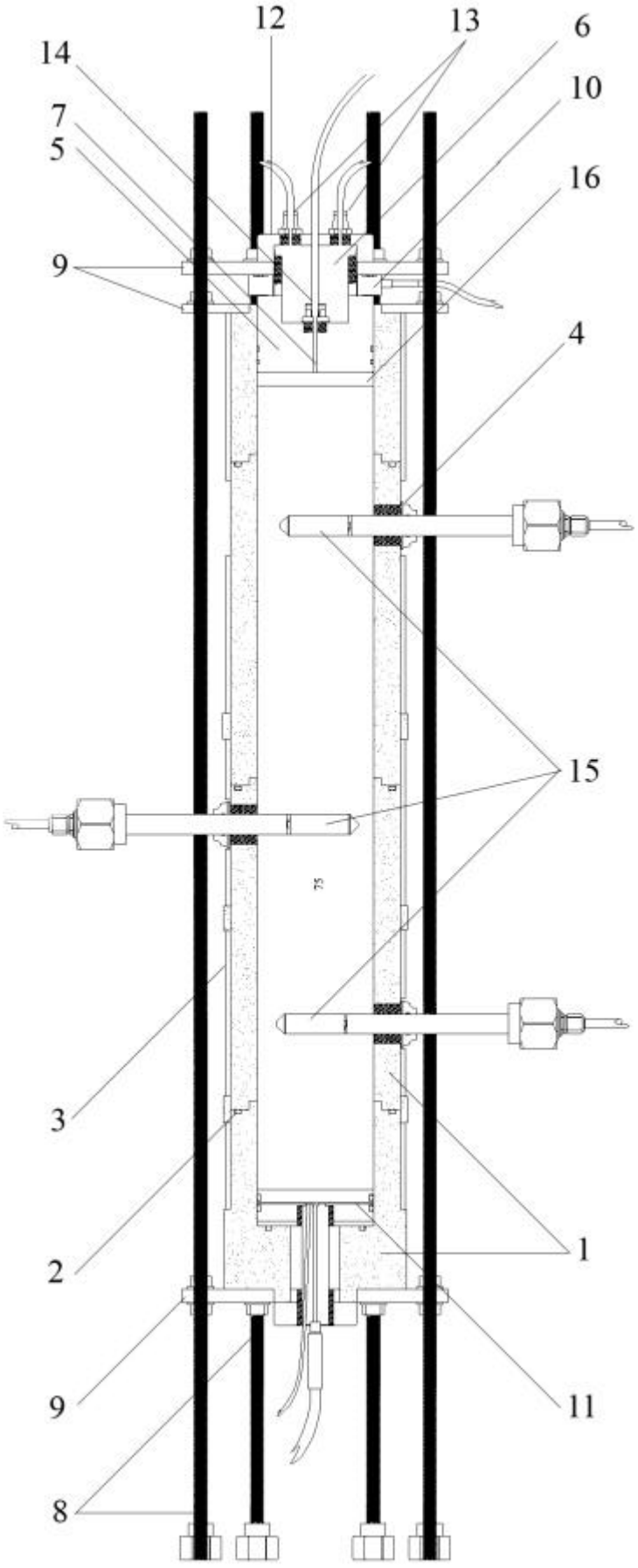


**Figure 7: Cross section of the cells with its different components**

## 3.2 HEATING SYSTEM

The heating system, inserted at the Teflon bottom of the cell, consists of several 316L stainless steel elements (Figure 7, item 11 and Figure 8).

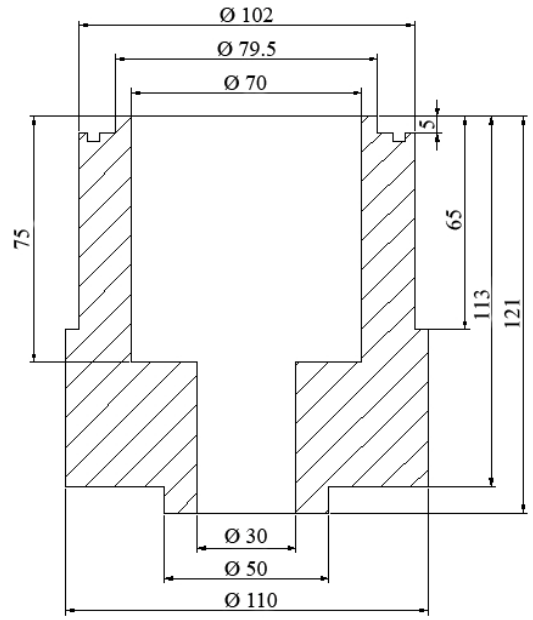


**Figure 8: Cross section of the Teflon base of the cell**

The electric heating element (Figure 9, item 2), a resistance of 30 W at 24 VAC, is sandwiched between two circular plates that press it, being its lower part insulated, and the upper one treated with a conductive paste to better transmit the heat towards the steel in contact with the bentonite. This set is sealed by lateral o-rings, and is pressed against the base of the cell by means of a piston rod threaded in it (Figure 9, item 5), which is tightened by means of a knurled nut in the outside of the cell (Figure 9, item 6). The cables of the control K-type thermocouple and of the power supply pass through the piston rod (Figure 9, right).

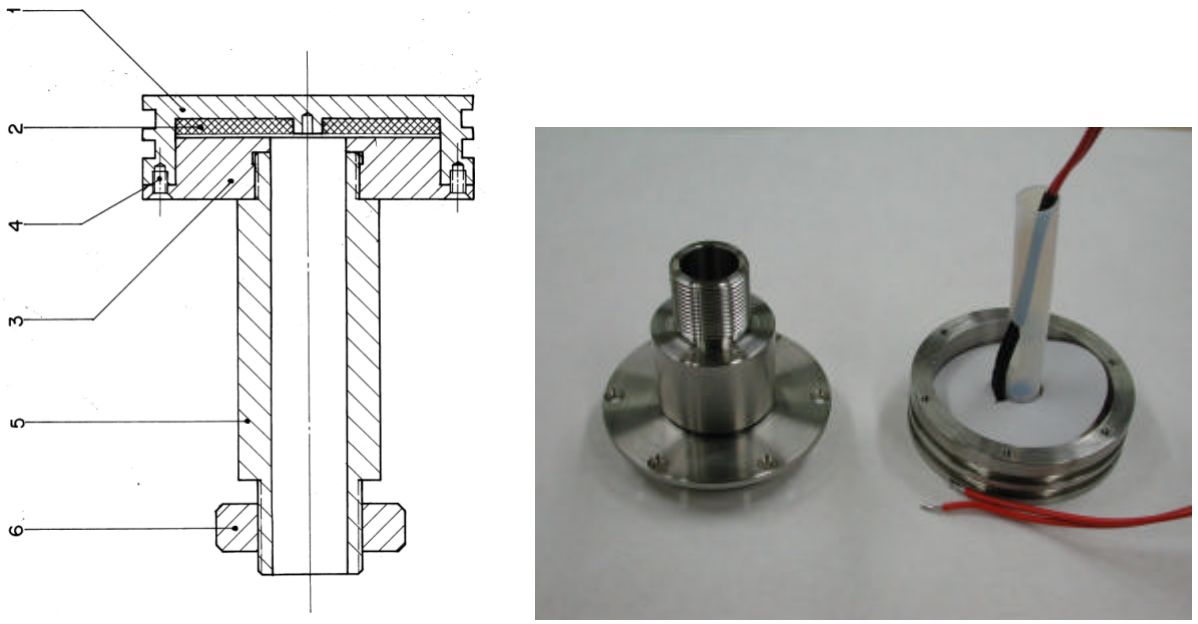


**Figure 9: Cross section (left) and appearance of the disassembled heating system (right)**

The temperature control is achieved by means of a microprocessor-based PID temperature controller CROUZET CTD46 that regulates a solid state relay, enabling or disabling the power output towards the resistance, according to the temperature reached. The controller has a function of automatic PID regulation that remains activated. The average power supplied to the resistance is measured by a ZIMME (model LMG95) precision power meter every 3 minutes. The value of the power supplied is sent to the data acquisition system, which communicates with the control PC through a GPIB interface.

## 3.3 COOLING SYSTEM

The upper plug of the cell is also a cooling chamber (Figure 7, item 6 and Figure 10) of an approximated volume of 45 $cm^3$, closed by a screwed cap (Figure 7, item 12). Deionised water at laboratory temperature is impelled and circulated by an EHEIM 1048 centrifugal pump through two holes with connections (Figure 7, item 13) drilled on the upper cap. In this cap there is also a perforation for the hydration system, as it is explained below.

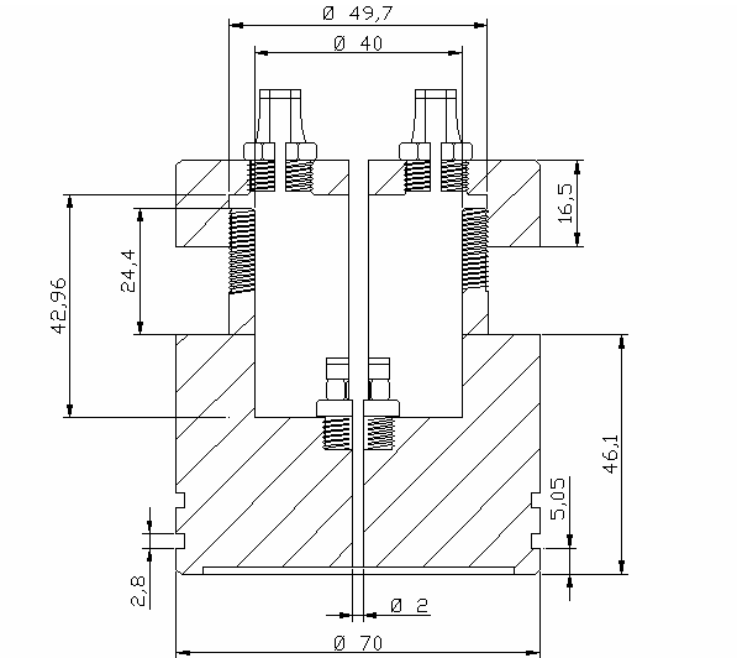


**Figure 10: Cross section of the upper steel plug with the cooling chamber**

## 3.4 HYDRATION SYSTEM

The hydration water is injected to the cells through the upper hydration line (Figure 7, item 14) that crosses the upper steel plug (Figure 10). This plug has concentric grooves machined on its bottom to help a better water distribution, what is further facilitated by the use of a porous filter placed on top of the sample. The hydration water used is a synthetic saline water (Pearson), which is a sodium-rich solution and has a composition similar to the Opalinus Clay formation pore water (Table I). The water is taken from a low pressure bladder accumulator manufactured in stainless steel by OLAER (EBV 1L-40B/00). The deposit has 1 L of capacity and can be recharged and pressurized with nitrogen up to 40 bar. The inlet valve is detached to connect the bladder to atmosphere. The deposit is filled by counter-pressure and the bladder is deformed elastically. Initially the injection pressure came from the elastic behaviour of the rubber bladder. This value was approximately 0.1 bar, since the deposits were not pressurised. The hydration circuit is equipped with valves that allow cutting off the water supply to the cell in order to avoid the system discharge in case of failures or modifications.

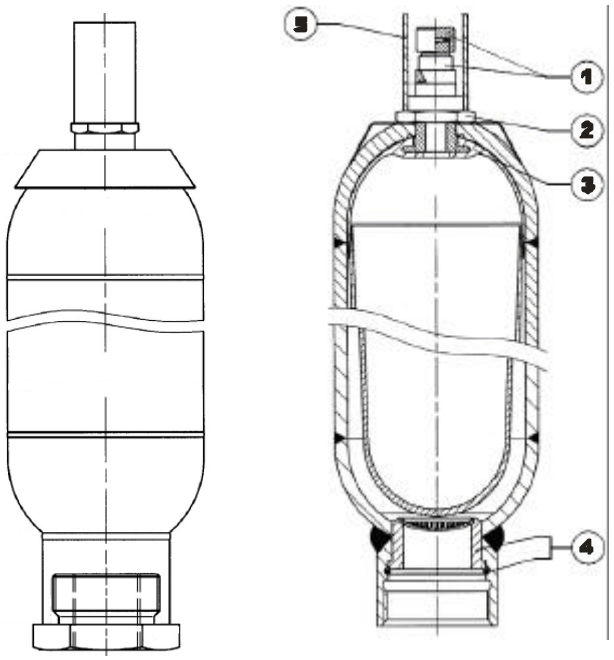


1. Gas inlet valve assembly
2. Nut
3. Bladder
4. Grid with spring ring
5. Protective cap

**Figure 11: Pressure bladder accumulator used as deposit and pressurising system for the hydration water**

## 3.5 INSTRUMENTATION

The water volume intake, the heater power, the axial pressure (in cell B), and the relative humidity (RH) and temperature (*T*) at different levels inside the clay are being measured as a function of time.

The cells are instrumented with capacitive-type sensors placed inside the clay at three different levels (10, 22 and 40 cm from the heater approximately) (Figure 7, item 15). The transmitters used are VAISALA HMT334 (Figure 12), which include a humidity sensor (HUMICAP®) that changes its dielectrical characteristics with extremely small variations in humidity (capacitive-type RH sensor). They include also a temperature sensing element (Pt 100). The accuracy of the humidity sensor is ±1% over the range 0-90 percent RH and ±2% over the range 90-100 percent RH. The transmitters are protected by cylindrical stainless steel filters.

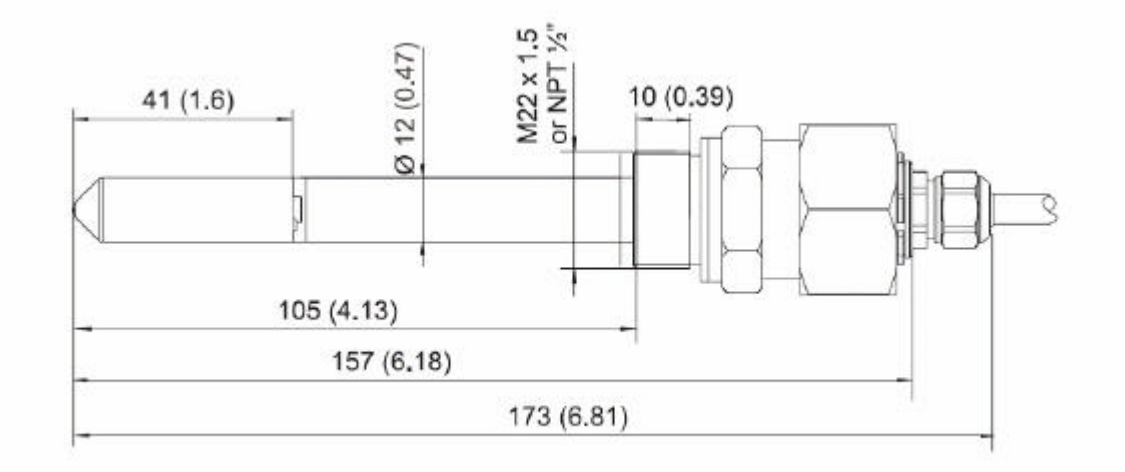


**Figure 12: Vaisala HMT334 relative humidity sensors**

The water intake is measured by changes in the weight of the deposits by means of an electronic load cell measurement system (Figure 13). The bottle is hanging from the load cell. The equipment consists of a load cell HBM (SP4MC6MR) with capacity of 7 kg and precision of 0.001 kg, connected to the amplifier for weighing application (HBM -MVD 2510- with analog output).

**Figure 13: Water deposits and load cells**

Cell B is instrumented with a ring load cell to determine the axial pressure generated during the test (Figure 14). This ring is located between the upper plug of the cell and the upper plate (Figure 6, right; Figure 7, item 10). The load cell ring is a LC8313-200-5K model by Omegadyne (Thru Hole Load Cell, 3.13" OD, 2.00" ID, 0-5,000 lb capacity (2268 kg)) measured with a Digital Panel Meter for Load Cell or Strain Gauge with analog output (OMEGA DP25B-S-230-A). It is made of stainless steel and has an accuracy of ±0.5%.

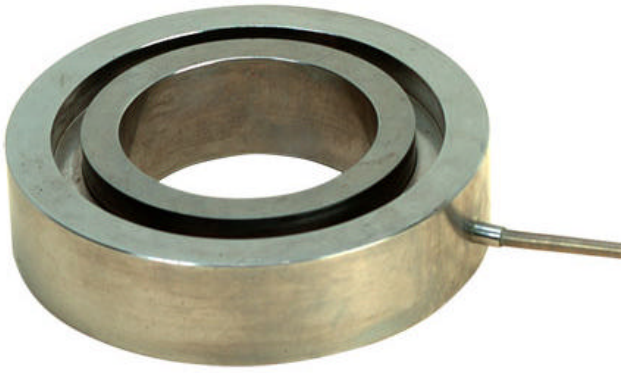

**Figure 14: Ring load cell used in cell B**

## 3.6 DATA ACQUISITION SYSTEM

The PC receives data from three types of sensors: relative humidity and temperature (RH/*T*), load cells and heater electric power supply.

All RH/T VAISALA transmitters are internally connected through a RS-485 serial line. An ADAM-4017 analog input module (16-bit, 8-channel) offers signal conditioning, A/D conversion, ranging and RS-485 digital communication functions for the values coming from the three load cells (Figure 15). An ADAM-4060 Relay Output Module acts as a low-power switching (ON/OFF control) of the VAISALA transmitters in case of blocking of the data line. Finally, two isolated RS-232 to RS-422/485 transmit the data to the computer system originally equipped with RS-232 (or multiple RS-232 to USB).

The power for the ADAMs modules and the VAISALA transmitters is supplied by two serial-connected TRACO POWER TCL 060-112 power sources (Figure 15).

The measurement of the power supplied to the heater is periodically integrated by a precision power meter ZIMMER LMG95 and values are directly sent to the computer through a GPIB interface.

LabVIEW was used to develop the data acquisition application. This application allows the configuration of different parameters for each experiment, asks for the data to the different nodes, shows the data in screen and records them in files. The parameters to be preset are: the sensors that take part in the experiment, the recording time, a threshold variation value that allows the acquisition of data if there is a significant variation, and the data file name. Once the experiment is launched, the program asks continuously for data and shows them in a graph. Periodically, or when there is an important change in any sensor, the data are saved into the selected file. Data acquisition goes on until user interaction.


**Figure 15: Data acquisition modules and their power supply**

## 3.7 EXTERNAL INSULATION

The cells are laterally surrounded with insulation. Initially, the material used was a 5-mm thick dense foam, whose thermal conductivity is 0.04 W/m·K. This was placed 7 h after the start of heating in cell S/B and from the beginning of heating in cell B. The sensors were also wrapped. Due to the lateral heat loss observed in this first stage, the foam was changed in column S/B

after 1566 h of heating by a 30-mm thick insulation wool (Superwool 607 HT Blanket) whose thermal conductivity is 0.04 W/m·K and a 25-mm thick ISOVER BT-LV insulation (thermal conductivity of 0.034 W/m·K) around the 8 cm at the bottom of the column (installed after 1666 h of heating). In cell B this isolation configuration was set after 1518 h of heating, with the only difference that the ISOVER material covered just the 5 cm at the bottom of the column (Figure 16).

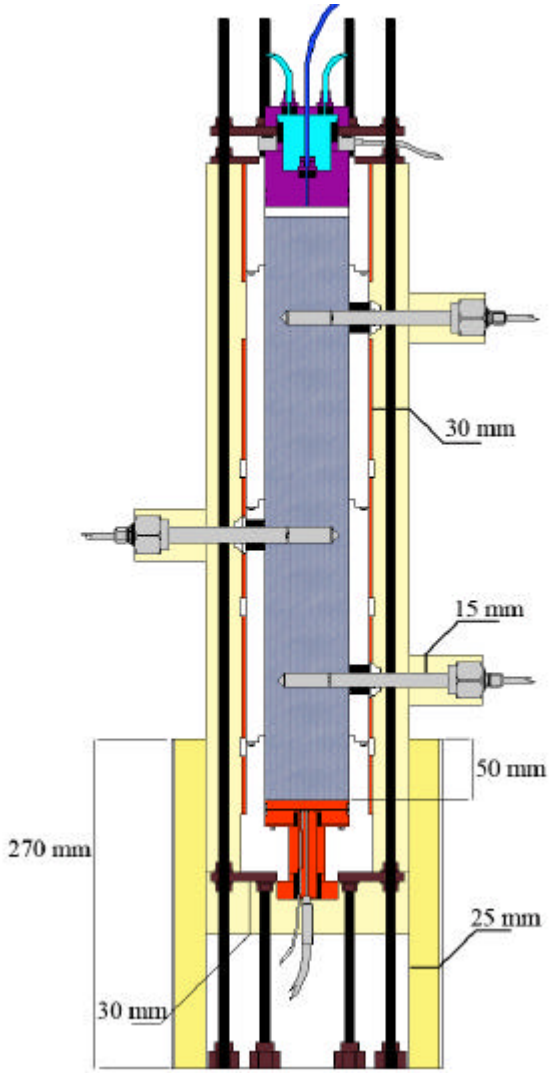


**Figure 16: Cell B with the external isolation**

# 4 Methodology

## 4.1 CELL ASSEMBLAGE AND FABRICATION OF THE COLUMNS

To assemble the cell, the Teflon base with the heater inserted and the cylindrical Teflon walls were first mounted (Figure 7, items 1 and 11). The columns were manufactured by filling the cells in seven 7-cm high layers. The material was just poured inside the cell. The quantity of material was computed taking into account the initial water content, the inner volume of the cells (7 cm in diameter and a target height of 50 cm) and the nominal dry density, which was 1.45 in the case of cell S/B and 1.47 in the case of cell B. To fill the pellets cell a funnel was used to avoid the loss of the finer particles (Figure 17, left). No compaction energy was needed to manufacture the bentonite pellets column, whereas a very low energy was applied to the

mixture: 5 to 10 strokes with a 2.5-kg Proctor rammer with a 30.5 cm drop to each of the 7 layers (Figure 17, right).

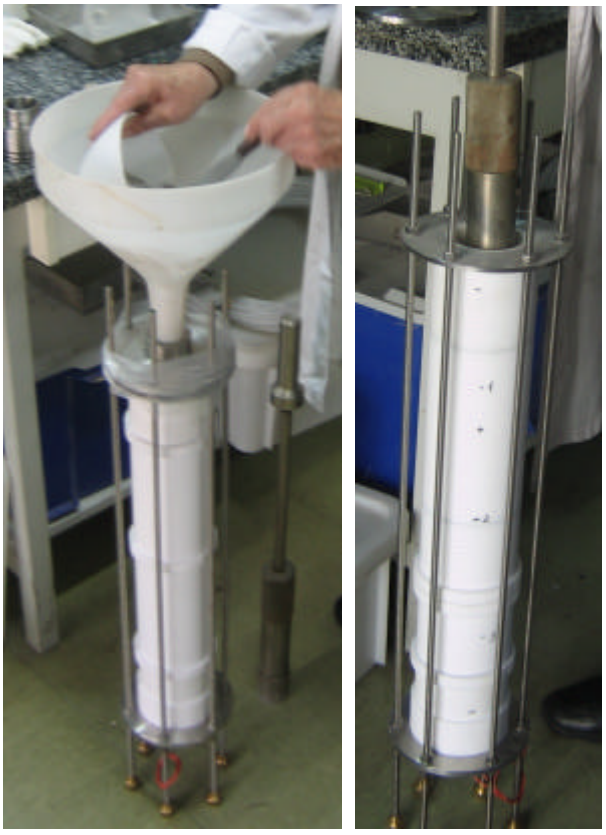

**Figure 17: Pouring of the pellets granulate inside the cell (left) and compaction of the S/B mixture (right)**

Between the clay and the upper closing, a 70-mm diameter and 8-mm high porous stone was placed (Figure 7, item 16). The top plug with the o-rings around (Figure 7, item 5) was pushed to its place and tightened. This assembly was weighed and afterwards, the perforations for the insertion of the sensors were drilled in the bentonite through the Teflon walls (Figure 18). The assembly was weighed again in order to know how much material had been lost as a consequence of drilling. Thus the initial characteristics of the columns were obtained (Table II). The differences with respect to the target values are due to the compression of the column caused by the upper plug tightening.

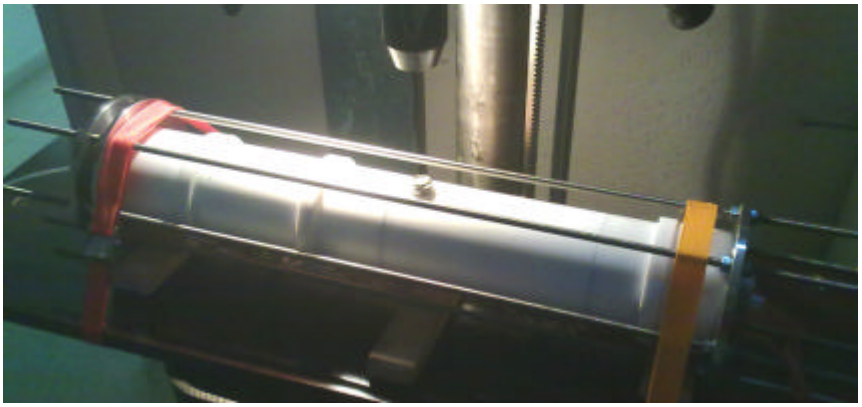

**Figure 18: Drilling of perforations in the Teflon and the sealing material for the insertion of sensors**

**Table II: Characteristics of the samples after compaction**

| | S/B | B |
|---|---|---|
| Initial water content (%) | 3.6 | 6.4 |
| Sample mass (g) | 2949 | 3094 |
| Sample mass after drilling (g) | 2930 | 3076 |
| Volume of sensors ($cm^3$) | 18 | 20 |
| Theoretical dry mass (g) | 2828 | 2891 |
| Diameter (mm) | 70.7 | 70.0 |
| Height (mm) | 494.6 | 483.9 |
| Dry density ($g/cm^3$) | 1.45 | 1.53 |
| Porosity | 0.463 | 0.444 |
| Void ratio | 0.863 | 0.797 |
| Degree of saturation (%) | 11 | 22 |

**Figure 19: Cell B before being wrapped with the insulation material (left) and THM cells in operation (right)**

The sensors were inserted in the bentonite at three different levels: at 10, 22 and 40 cm from the heater. The middle part of the stainless steel filter of each sensor was located approximately in the central vertical axis of the columns (see Figure 12). The holes in the cell walls were sealed by plugs with o-rings placed in contact with the sensors. Afterwards, the upper cooling chamber was closed and the injection tube on the upper part of the cell was connected to the water supply system, with the valve closed. All the sensors were connected to the data acquisition system. Then, the body of cell B was covered with the steel pieces tightened with steel braces (Figure 19, left) and finally the cell and sensors were covered with the isolation material. Figure 19 (right) shows the aspect of the cells in its final configuration.

## 4.2 TESTS INITIATION

Once the cell was mounted and the sensors inserted, the data acquisition was launched. A brief period to check the initial stabilisation and the correct working of the sensors was taken. This period lasted 140 hours for cell B and 260 h for cell S/B. The values recorded by the sensors during this period are shown in Figure 20 for cell S/B and in Figure 21 for cell B. The temperatures recorded by the three sensors in each cell were nearly identical and reflected the laboratory changes. For the relative humidity the differences inside the same column were below 1%, with average values of 40% in cell B and 46% in cell S/B.

Accidentally, the valve giving access to hydration was opened in cell S/B for a few minutes (about 5 min), and due to the high permeability of the material, this caused the relative humidity in the upper part of the column to increase. This is why sensor 1 recorded a steady increase until a value of 52%, while the other two recorded an increase of about 0.5%. The average water content of the column increased from 3.6 to 4.7%.

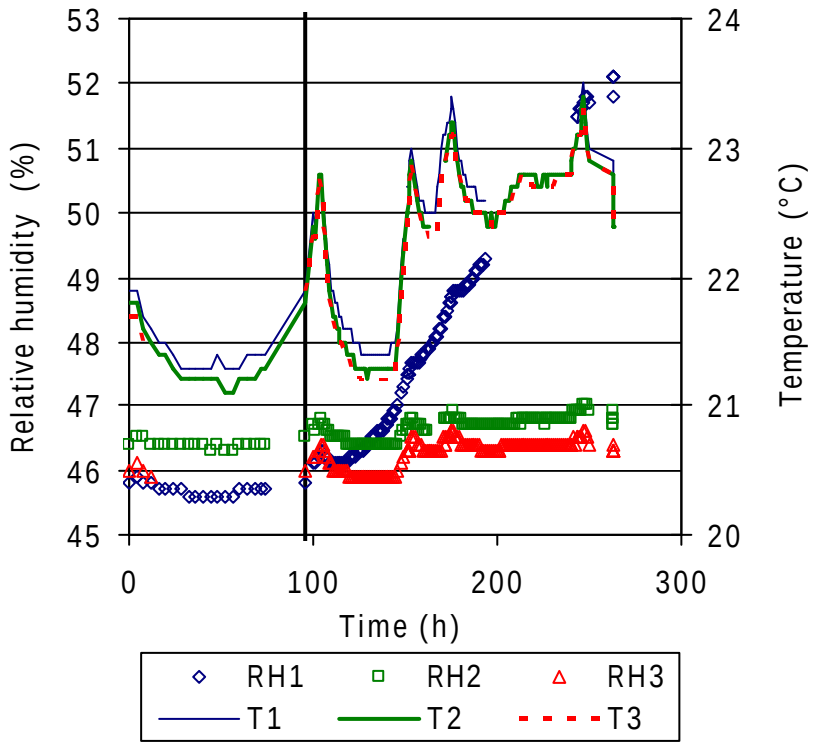


**Figure 20: Sensors readings before initiation of the test in Cell S/B (sensor 1 placed at 40 cm from the bottom, sensor 2 at 22 cm and sensor 3 at 10 cm). The thick vertical line indicates the accidental opening of the hydration line**

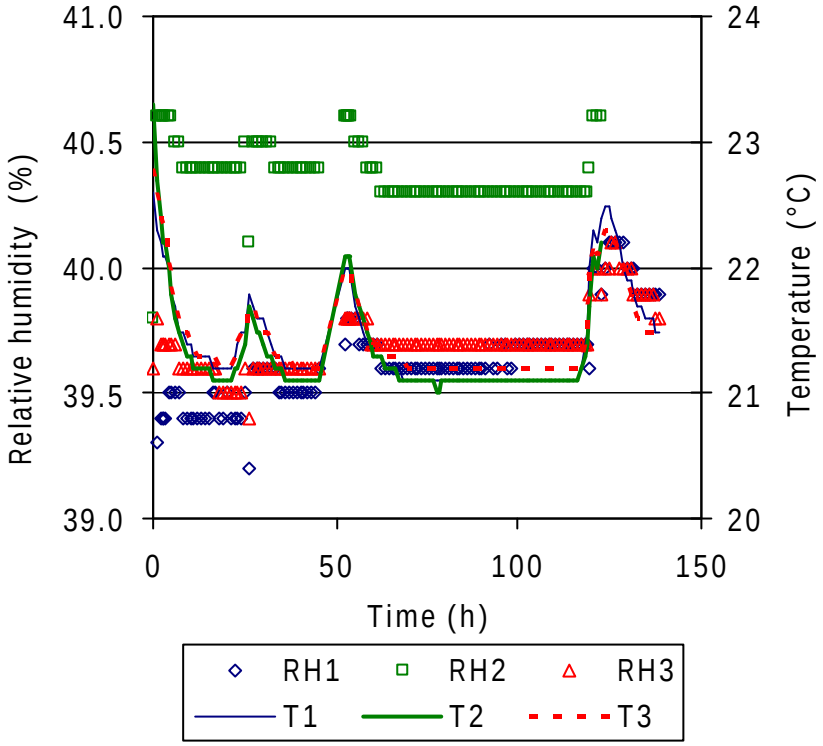


**Figure 21: Sensors readings before initiation of the test in Cell B (sensor 1 placed at 40 cm from the bottom, sensor 2 at 22 cm and sensor 3 at 10 cm)**

# 5 Results

## 5.1 CELL S/B

### 5.1.1 Initial heating

In the case of the test performed with the sand/bentonite mixture (cell S/B), 260 h after starting data acquisition the heater temperature was set at 100°C and the cooling system on top kicked off, and this time is considered as *t*=0 for the rest of the test. The target temperature was reached in 25 min, but the stabilisation of the temperature registered by the sensors took approximately 30 h, and much longer for the relative humidity (Figure 22). After 7 h of heating the cell was wrapped with an isolating material (see section 3.7) and this was clearly reflected in an increase of the temperature inside the mixture and affected as well the relative humidity.

After 1566 h the isolation material was changed, and again modified after 1666 h (see section 3.7 for details), what improved the longitudinal heat transmission inside the column and caused a temperature increase of almost 10°C at 10 cm from the heater (sensor 3) (Figure 23, left). As well, the laboratory temperature changes were subsequently less reflected in the temperatures inside the material. The relative humidity inside the cell also reflected the improvement of the isolation system and the ensuing increase of temperature in the mixture (Figure 23, right). The two sensors farther from the heater reflected an increase in relative humidity from the beginning of heating, more intense for the middle sensor from the moment the temperatures near the heater increased. Both sensors recorded a stable and similar RH value approximately after 2200 h. However, the sensor placed at 10 cm from the heater recorded a sharp initial increase up to a value of RH 70%, but after 120 h it started to decrease, more intensely when the isolation was improved. A quasi-stable value of 36% was reached after 2400 h. This

evolution of the relative humidity along the column reflects the migration of water in the vapour phase from the material close to the heater towards cooler zones.

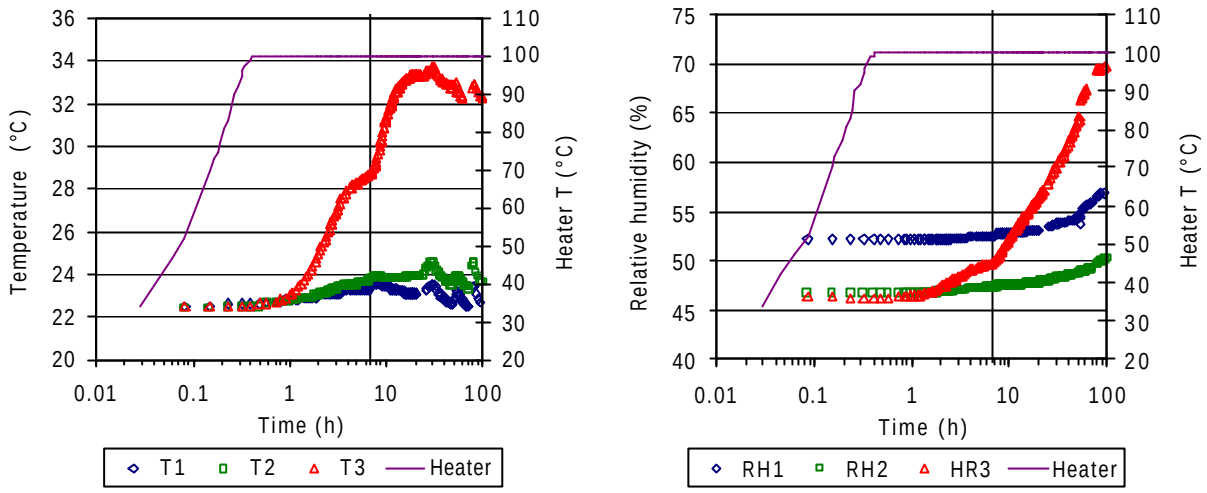


**Figure 22: Evolution of *T* and RH in cell S/B after switching on the heater at 100°C (sensor 1 placed at 40 cm from the bottom, sensor 2 at 22 cm and sensor 3 at 10 cm). The thick vertical line indicates the wrapping of the cell with the first isolating material**

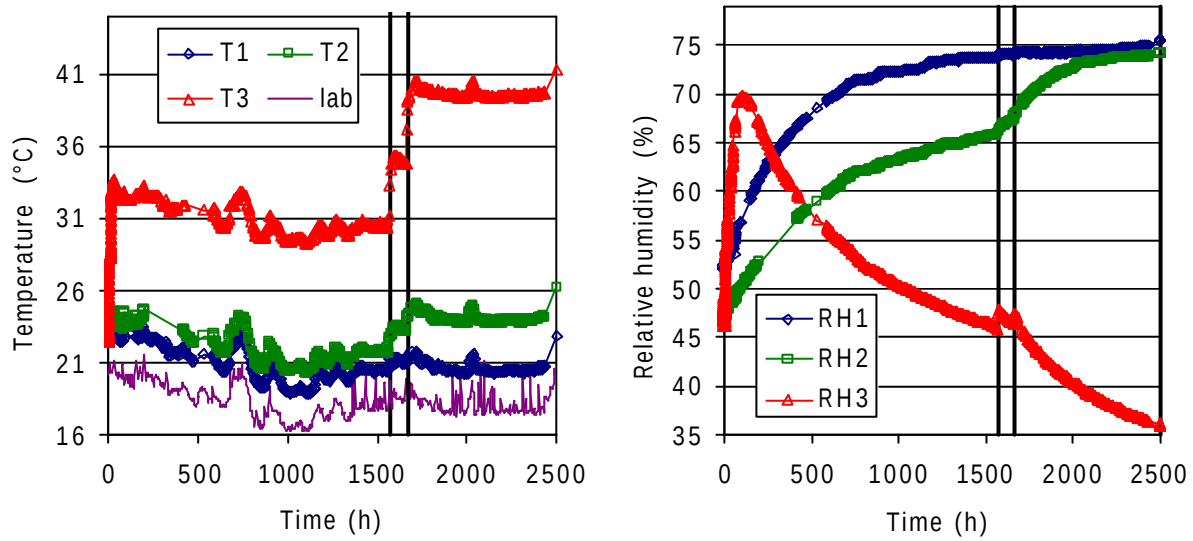


**Figure 23: Evolution of *T* and RH in cell S/B during the phase in which the heater was set at 100°C (sensor 1 placed at 40 cm from the bottom, sensor 2 at 22 cm and sensor 3 at 10 cm). The thick vertical lines indicate improvements in the isolation system**

Once the relative humidity inside the column stabilised, the heater temperature was increased to 140°C, final target temperature, in 12 min. The temperatures inside the mixture stabilised after 24 h, and the relative humidity in approximately 1130 h (Figure 24).

The equilibrium values of *T* and RH at the end of this phase and of the previous phase with heater at 100°C are shown in Figure 25. A summary of the values recorded during the whole heating phase is given in Table A- I and Table A- II in Appendix 1.

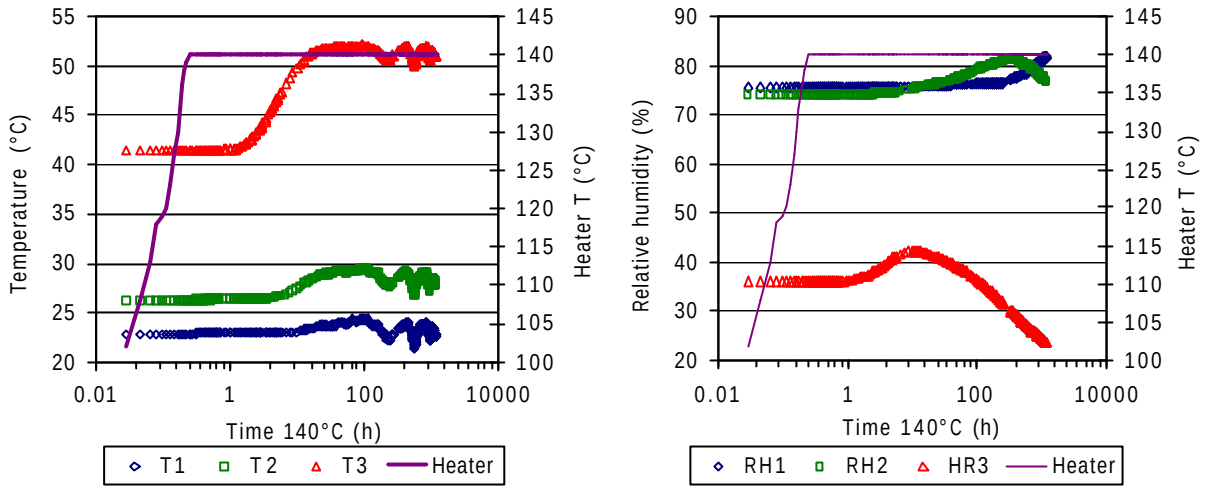


**Figure 24: Detailed evolution of *T* and RH in cell S/B as the heater *T* increased from 100 to 140°C (sensor 1 placed at 40 cm from the bottom, sensor 2 at 22 cm and sensor 3 at 10 cm)**

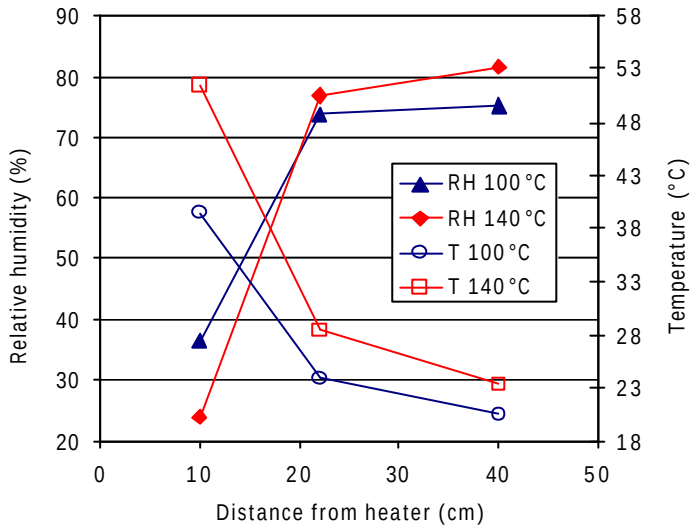


**Figure 25: Equilibrium values for heater temperatures of 100°C (*t*=2400 h) and 140°C (*t*=3620 h) in cell S/B**

### 5.1.2 Heating and hydration

After the stabilisation of RH and *T* for a heater temperature of 140°C, the hydration line was opened at a pressure of approximately 0.1 bar.

Figure 26 shows the evolution of *T* and RH recorded by the sensors after the beginning of hydration. The temperatures kept the same as before hydration for some days. As the water front approached the sensors, the temperatures started to increase, so the simultaneous increase in temperature and relative humidity took place first in sensor 1 (after approx. 44 h), then in sensor 2 (after approx. 160 h) and finally in sensor 3 (after approx. 235 h). The coupling between the increase in water content and that of temperature can be clearly seen in Figure 27. For sensor 3, placed in the hottest area, the arrival of the water front caused a temporary decrease in temperature that was quickly recovered. The overall increase in temperature due to the increase of water content was of 6°C for sensor 1, 14°C for sensor 2 and 16°C for sensor 3.

With respect to the RH evolution, its increase was very sudden once the water front reached the area where the sensors were placed. Consequently the sensors became quickly flooded and started recording faulty values (except for sensor 1 which records a RH value of 98%). Sensor 1 started recording 98% approximately 135 h after hydration started, sensor 2 after 235 h and sensor 3 after 387 h. The overall water intake was also very large until the bottom sensor became flooded, and then the water intake rate softened (continuous line in Figure 26, right). In fact, air bubbles could be seen in the hydration line, and these were periodically purged, since they seemed to hinder the water inflow. This is the reason why the water intake curve is not smooth, because after purging the water intake was temporarily accelerated. According to the water intake measurements, after 1655 h of hydration the overall water content of the mixture was 28% and its degree of saturation 88%.

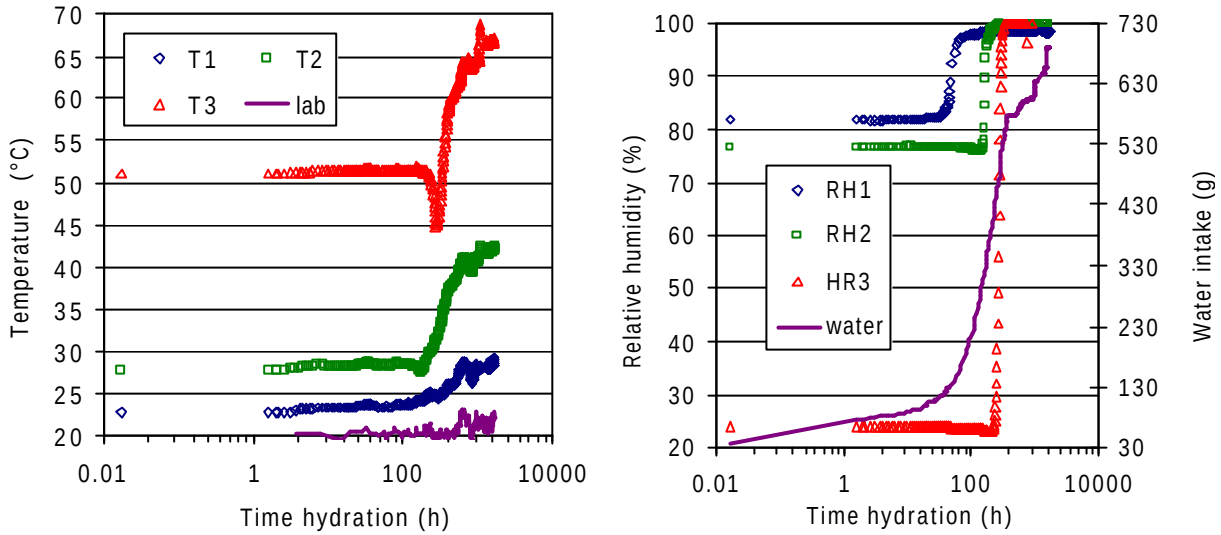


**Figure 26: Evolution of *T* (left) and RH (right) in cell S/B after the beginning of hydration (sensor 1 placed at 40 cm from the bottom, sensor 2 at 22 cm and sensor 3 at 10 cm)**

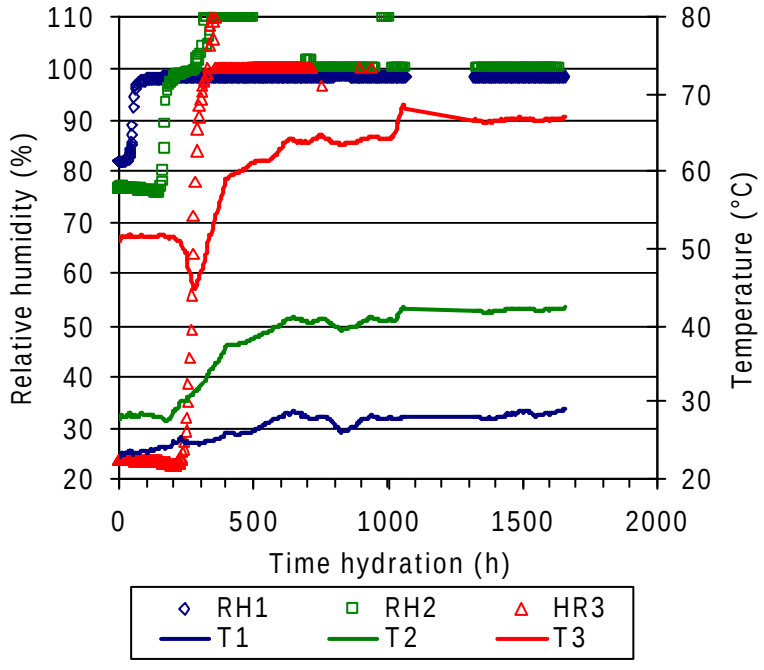


**Figure 27: Evolution of *T* and RH in cell S/B after the beginning of hydration (sensor 1 placed at 40 cm from the bottom, sensor 2 at 22 cm and sensor 3 at 10 cm)**

The heater power was also measured during all the test phases (except for the first 80 h) and the values are plotted in Figure 28, along with the temperature inside the mixture at 10 cm from the heater. The improvement of the isolation induced a decrease of the heater power from 10.7 to 6.6 W to keep the target temperature of 100°C at the heater surface. When the heater temperature was increased to 140°C, the heater power increased to 10 W. Upon hydration, the arrival of water to the heater area (marked by a decrease followed by an increase of temperature recorded by sensor 3) gave place to a progressive increase of heater power up to a value of 12 W.

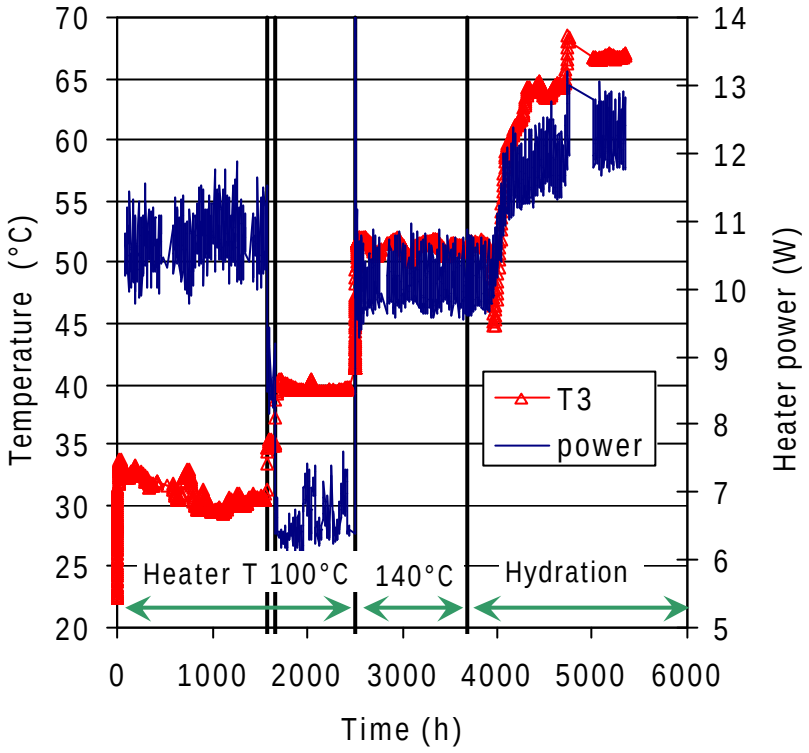


**Figure 28: Heater power and temperature at 10 cm from the heater (sensor 3) in cell S/B during the test (the two first thick vertical lines indicate the improvement of isolation)**

## 5.2 CELL B

### 5.2.1 Initial heating

In the test performed with the bentonite pellets (cell B), 160 h after starting data acquisition the heater temperature was set at 100°C and the cooling system was kicked off, and this time is considered as *t*=0 for the rest of the test. The target temperature was reached in 33 min, but the stabilisation of the temperature registered by the sensors took approximately 20 h, and much longer for the relative humidity (Figure 29). During the first 25 hours the intermediate sensor values were not recorded.

The isolation was reinforced 1500 hours after heating started (see section 3.7 for details), and the temperature inside the bentonite increased, mainly close to the heater, sensor 3 recording an increase of almost 10°C (Figure 30, left). As well, the laboratory temperature changes were less reflected in the temperatures inside the material once isolation was improved. The relative humidity inside the cell also reflected the improvement of the isolation system and the subsequent increase of temperature in the bentonite (Figure 30, right). At 10 cm from the heater (sensor 3) the relative humidity increased sharply during the first 300 h, and then started to decrease. The improvement of the isolation gave place to a sudden new increase

followed by a new decrease, at a different pace, down to quasi-equilibrium values of 34% after approximately 3500 h. In the middle of the column heating triggered a continuous increase in relative humidity up to an equilibrium value of 55% that was attained after 2400 h. At 40 cm from the heater it took almost 1000 h of heating for the relative humidity to increase, what points to a slow movement of the water vapour phase. After 3600 h of heating this value was still lower than in the central part of the column.

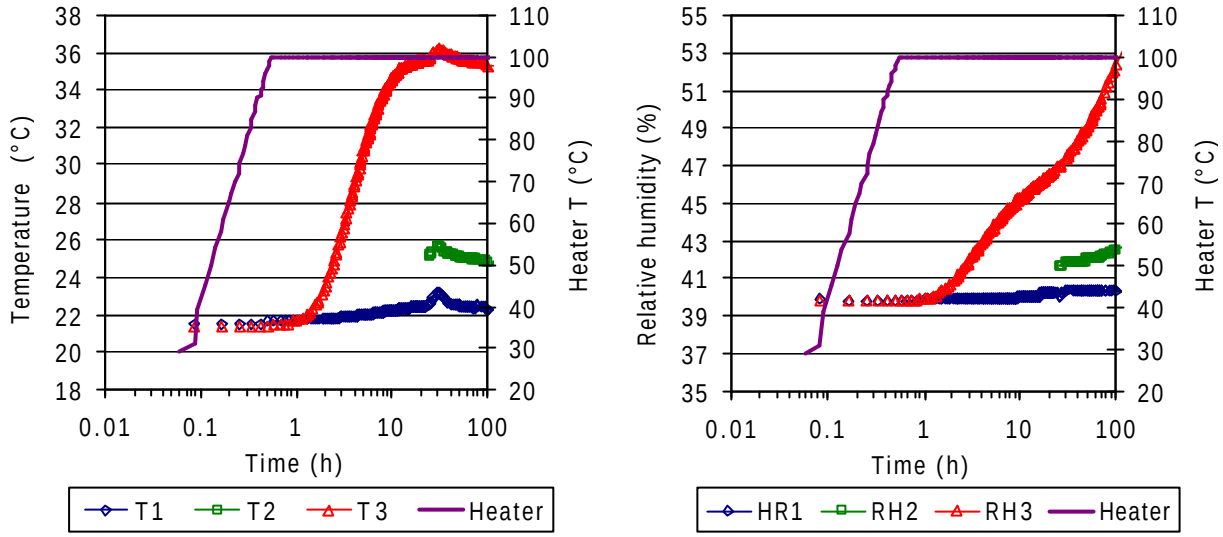


**Figure 29: Initial evolution of *T* and RH in cell B after switching on the heater at 100°C (sensor 1 placed at 40 cm from the bottom, sensor 2 at 22 cm and sensor 3 at 10 cm)**

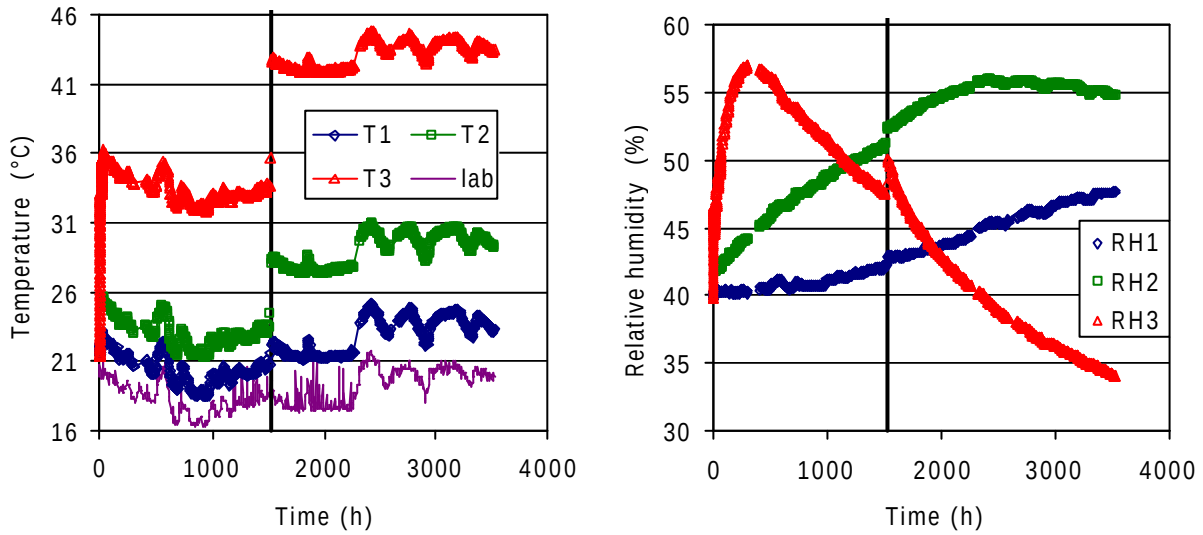


**Figure 30: Evolution of *T* and RH in cell B during the phase in which the heater was set at 100°C (sensor 1 placed at 40 cm from the bottom, sensor 2 at 22 cm and sensor 3 at 10 cm). The thick vertical lines indicate improvements in the isolation system**

Once the relative humidity inside the column stabilised, the heater temperature was increased to 140°C, final target temperature, in 17 min. The temperatures inside the mixture stabilised after 35 h, and the relative humidity in 1500 h (Figure 31). The equilibrium values of *T* and RH at the end of this phase and of the previous phase with heater temperature at 100°C are shown in

Figure 32 and a summary of the values recorded during the initial heating is given in Table A- III and Table A- IV in Appendix 1.

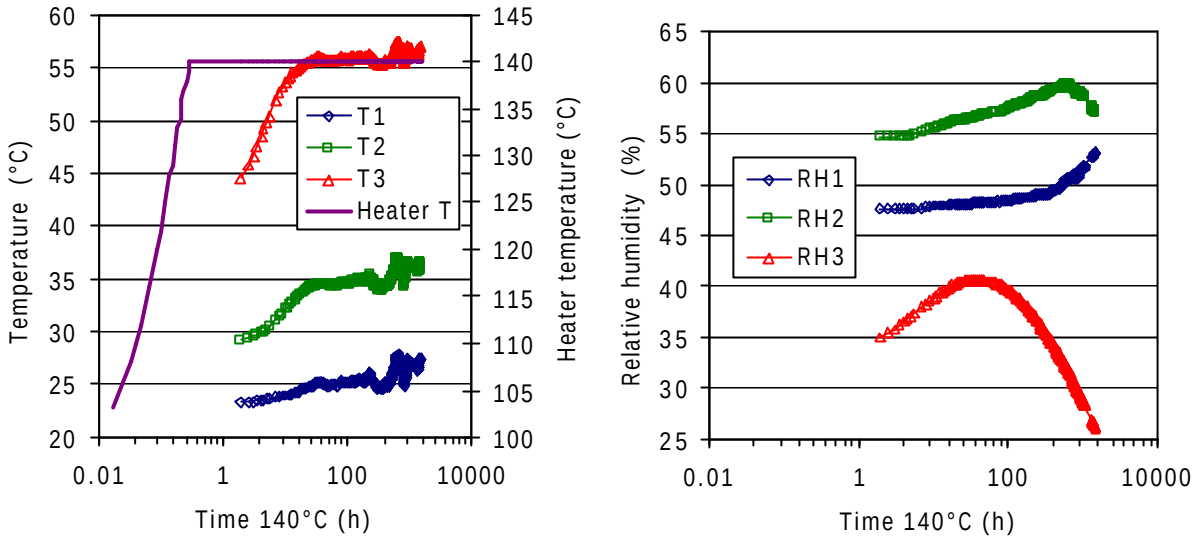


**Figure 31: Detailed evolution of *T* and RH in cell B as the heater *T* increased from 100 to 140°C (sensor 1 placed at 40 cm from the bottom, sensor 2 at 22 cm and sensor 3 at 10 cm)**

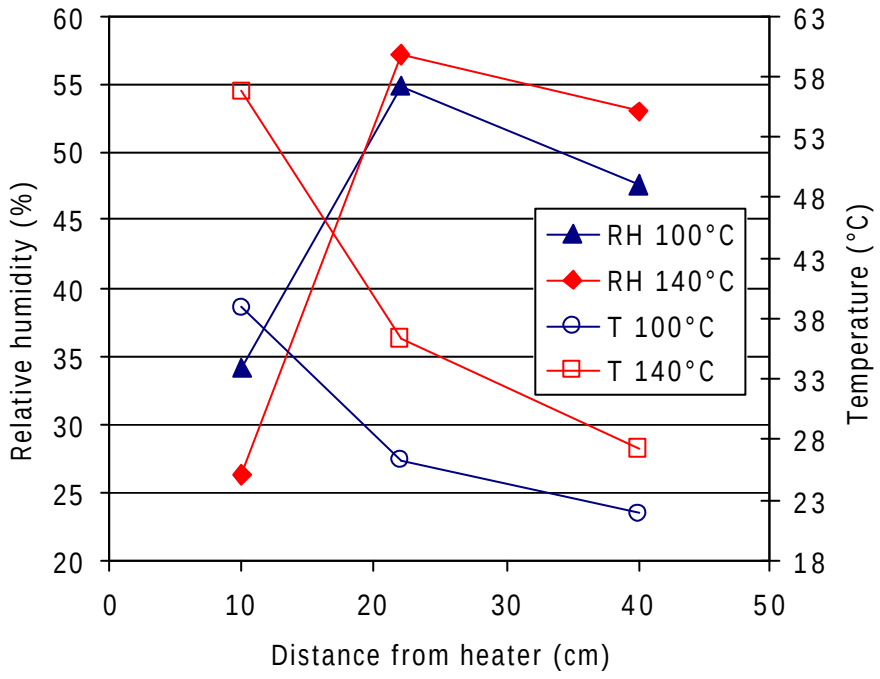


**Figure 32: Equilibrium values for heater *T* of 100°C (*t*=3524 h) and 140°C (*t*=5015 h) in cell B**

In this cell the axial pressure was also measured on the top of the cell (see section 3.5 for details), and the values recorded are shown in Figure 33, where the temperature recorded by the upper sensor is also plotted. During the heating phase the pressure is clearly related to temperature, increasing with it. An average value of 0.1 MPa was recorded when the heater temperature was 100°C and of 0.15 MPa when the heater temperature increased to 140°C.

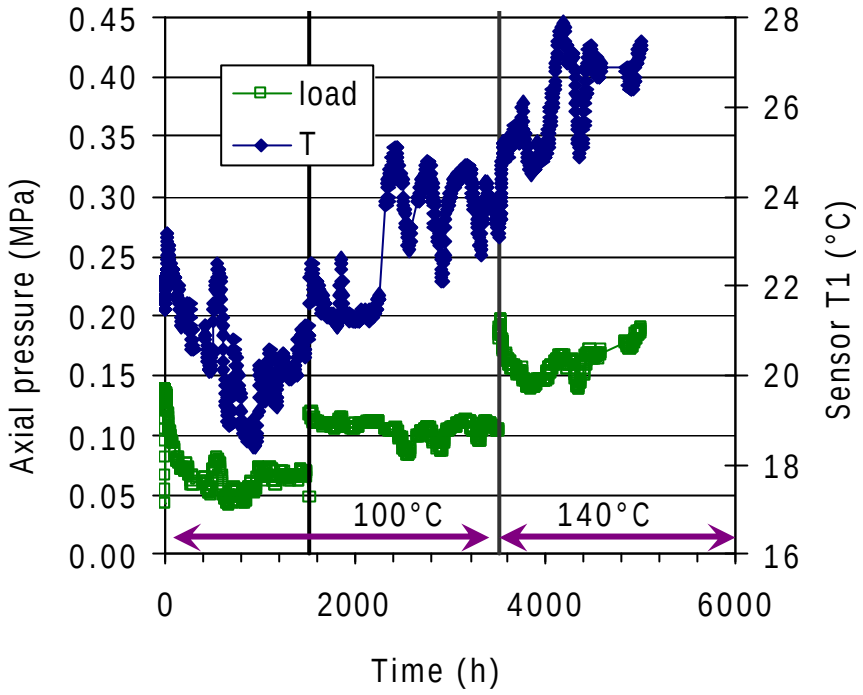


**Figure 33: Axial pressure on top and *T* at 10 cm from the upper surface (sensor 1) in cell B during the heating phase (the first thick vertical line indicates the improvement of isolation)**

### 5.2.2 Heating and hydration

After the stabilisation of RH and *T* for heater temperature of 140°C, the hydration line was opened at a pressure of approximately 0.1 bar.

Figure 34 shows the evolution of *T* and RH recorded by the sensors after the beginning of hydration. During the first 300 h both the temperatures and the relative humidity kept the same as before hydration. The overall water intake is also shown in the Figure (right).

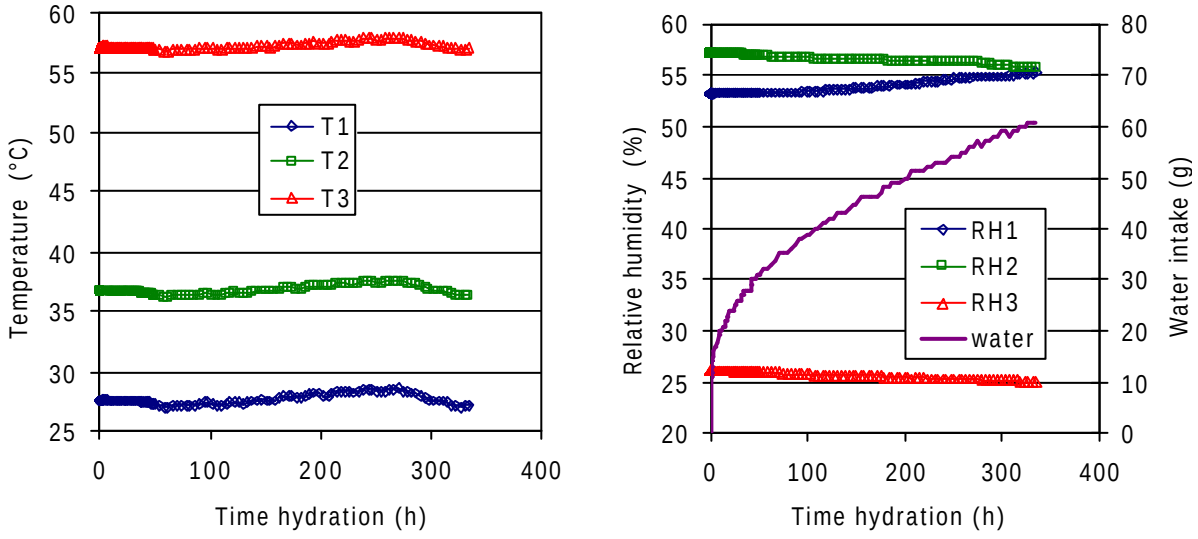


**Figure 34: Evolution of *T* (left) and RH (right) in cell B after the beginning of hydration (sensor 1 placed at 40 cm from the bottom, sensor 2 at 22 cm and sensor 3 at 10 cm)**

The heater power was measured during the test (except for the first 1250 h) and the values are plotted in Figure 35, along with the temperature inside the mixture at 10 cm from the heater (sensor 3). The improvement of the isolation induced a decrease of the heater power from 12 to 8 W to keep the target temperature of 100°C at the heater surface. When the heater temperature was increased to 140°C, the heater power increased to 12 W.

The axial pressure measured on top of the cell (see section 3.5 for details) and the water intake values are shown in Figure 36. Both seem to be correlated.

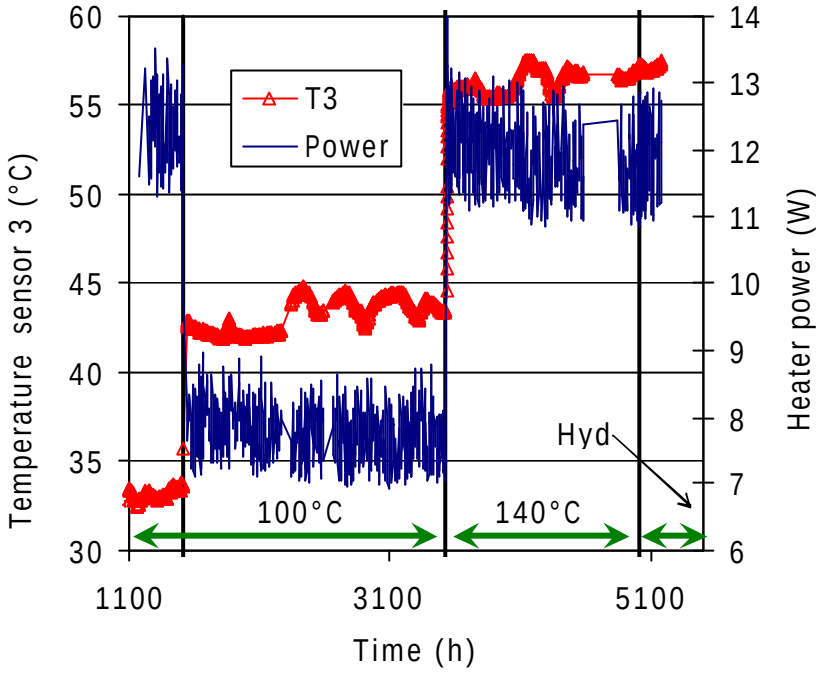


**Figure 35: Heater power and *T* at 10 cm from the heater (sensor 3) in cell B during the test (the first thick vertical line indicates the improvement of isolation)**

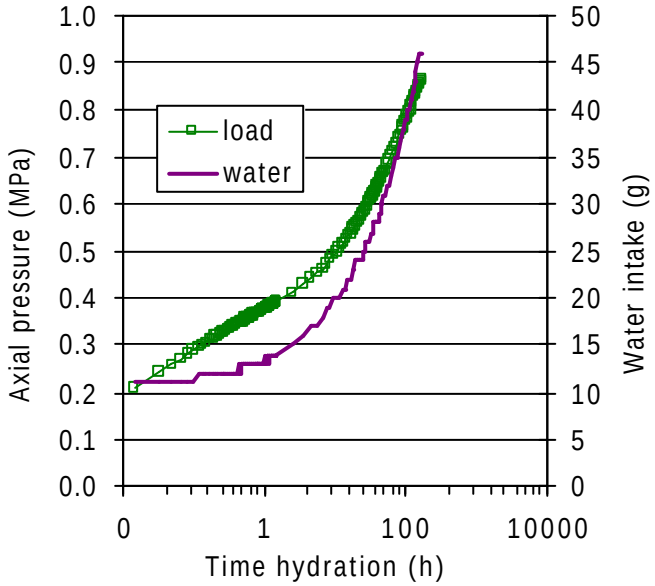


**Figure 36: Axial pressure measured on top of cell B and water intake from the beginning of hydration**

# 6 Summary and discussion

Figure 37 shows the equilibrium temperatures and relative humidities for the two tests for heater temperatures of 100 and 140°C before the start of hydration. The heating phase of both tests showed that the thermal conductivity of the dry materials is low, what causes the high difference in temperature between the heater surface and the sensor located at 10 cm, generating a high thermal gradient near the heater, and low temperatures in the rest of the columns. Besides, the stabilisation of the temperature in these materials is very quick, being faster in cell B than in cell S/B (Figure 22 and Figure 29). The presence in cell B of the steel reinforcement could be the responsible for the slightly higher temperature measured, despite the fact that the thermal conductivity of the sand/bentonite mixture (before compaction) is higher than that of the bentonite pellets. A reason for this difference could be that the thermal contact between the heater plate and the pellets is better than in the case of the mixture, due to the different granulometry of both materials, which is more heterogeneous for the pellets, allowing for a better filling of pores (Figure 3).

As well, the power needed to keep a given temperature at the heater surface was higher in cell B than in cell S/B (8 *vs*. 7 for heater *T*=100°C and 12 *vs*. 10 for heater *T*=140°C).

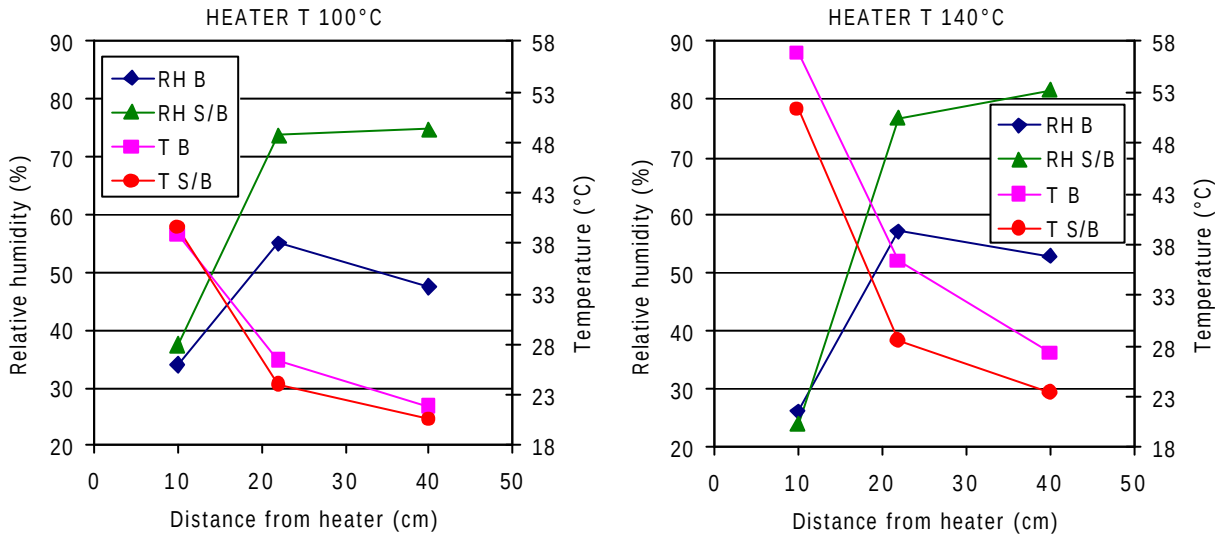


**Figure 37: Equilibrium *T* and RH before hydration in cells S/B and B for heater *T* 100 and 140°C**

The movement of water in the vapour phase as a result of the thermal gradient is evinced by the sharp increase of relative humidity recorded by the sensors closest to the heater –followed by a continuous decrease– and the slower increase recorded by the other two sensors (Figure 23 and Figure 30). The different permeability of both materials is made clear in the different pace and extent of this water redistribution process in the vapour phase. Thus, the initial increase of relative humidity at 10 cm from the heater was faster in cell S/B: when the heater was set at 100°C it took 120 h for the RH to reach a peak value of 70% in cell S/B and 300 h to reach a peak value of 57% in cell B. When the heater was set at 140°C it took just 11 h for the RH to reach a peak value at 10 cm from the heater (sensor 3) of 42% in cell S/B and 37 h to reach a peak value of 41% in cell B (Figure 24 and Figure 31). The relative humidity increase in the upper part of the column when the heater was set at 100°C started just after about 20 h in cell S/B and around 1000 h in cell B. Also the final relative humidity gradient is sharper in cell S/B than in cell B, due to the lower permeability and higher water retention capacity of the

bentonite pellets, which makes that before hydration, the higher relative humidity in cell B be recorded in the middle of the column (Figure 38).

The lower permeability of the pellets is again highlighted by the fact that after more than 300 h of hydration, the upper sensor in cell B had not yet recorded any RH change, while by this time the lower sensor in cell S/B had already recorded the arrival of the hydration front.

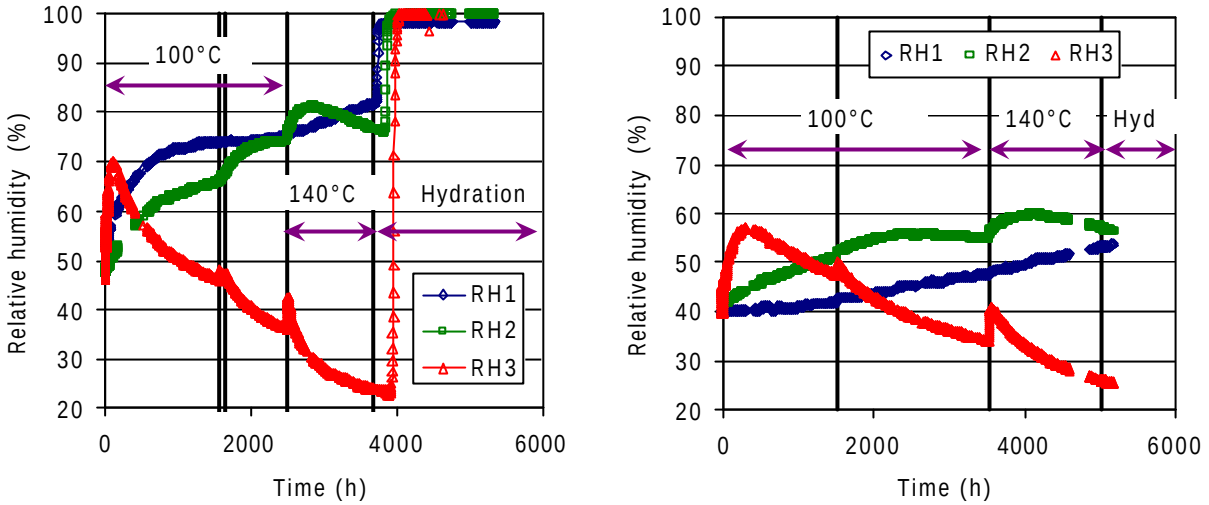


**Figure 38: Evolution of RH during the whole test in cell S/B (left) and cell B (right)**

# 7 References

ENRESA 2005. Ventilation experiment in Opalinus Clay for the management of radioactive waste. Publicación Técnica ENRESA 07/2005. Madrid, 82 pp.

Fernández, A.M. 2011. Determination of the Specific Heat Capa city of materials used as confinement barrier at El Cabril. Interim Report CIEMAT/DMA/2G208/3/11, 26 pp.

Gaus, I., Wieczorek, K., Mayor J.C., Trick T., García-Siñeriz, J.L., Schuster, K., Garitte, B., Kuhlman, U. 2011. EBS behaviour immediately after repository closure in a clay host rock: theHE-E experiment (Mont Terri URL). Proceedings of the 14th Int. Conference on Environmental Remediation and Radioactive Waste Management ICEM'11. September 25-29, 2011, Reims, France. P-59288. ASME, 7 pp.

Johnson, L.H ., Niemeyer, M., Klubertanz, G., Siegel, P., Gribi, P. (2002): Calculations of the temperature evolution of a repository for spent fuel, vitrified high-level waste and intermediate level waste in Opalinus Clay. Nagra Technical Report NTB 01-04. Nagra, Wettingen, Switzerland.

Pearson F., 1998. Artificial waters for use in laboratory and field experiments with Opalinus Clay *Paul Scherrer Institut. TM 44-98-08*

Pearson, F. J., Scholtis, A., Gautschi, A., Baeyens, B., Bradbury, M., And Degueldre , C. 1999. Chemistry of porewater in matrix and faults. – In: Thury, M. & Bossart, P. (Eds.), Mont Terri Rock Laboratory: Results of the hydrogeological, geochemical, and geotechnical experiments performed in 1996 and 1997.

Plötze M., Weber H.P (2007): ESDRED: Emplacement tests with granular bentonite MX-80: Laboratory results from ETH Zürich. Nagra Arbeitsbericht NAB 07-24. Nagra, Wettingen.

Teodori, S.P., Gaus, I. (Eds.) 2011. Long Term Performance of Engineered Barrier Systems (PEBS). Mont Terri HE-E experiment: as built report. Nagra Arbeitsbericht NAB 11-25. Nagra, Wettingen, 125 pp.

**Villar, M.V.**; Martín, P.L. & Barcala, J.M. 2005a. Infiltration tests at isothermal conditions and under thermal gradient. Informe Técnico CIEMAT/DMA/M2140/1/05. Madrid, 24 pp. Abril 2005.

Villar, M.V.; Martín, P.L. & Barcala, J.M. 2005b. Modification of physical, mechanical and hydraulic properties of bentonite by thermo-hydraulic gradients. Engineering Geology 81(3): 284-297.

Villar, M.V.; Sánchez, M. & Gens, A. 2008. Behaviour of a bentonite barrier in the laboratory: experimental results up to 8 years and numerical simulation. Physics and Chemistry of the Earth 33: S476-S485.

# Appendix 1 VALUES RECORDED BY SENSORS

**Table A- I: Relative humidity (RH) and temperature (*T*) recorded by sensors while the heater *T* was set to 100°C in cell S/B (sensor 1 placed at 40 cm from the bottom, sensor 2 at 22 cm and sensor 3 at 10 cm)**

| Time[a] (h) | Heater *T* (°C) | RH1 (%) | T1 (°C) | RH2 (%) | T2 (°C) | RH3 (%) | T3 (°C) |
|---|---|---|---|---|---|---|---|
| 0 | 22 | 52 | 22.5 | 47 | 22.4 | 46 | 22.4 |
| 1 | 100 | 52 | 22.7 | 47 | 22.6 | 46 | 23.0 |
| 2 | 100 | 52 | 22.9 | 47 | 22.9 | 47 | 24.9 |
| 5 | 100 | 53 | 23.2 | 47 | 23.5 | 49 | 28.3 |
| 10 | 100 | 53 | 23.4 | 47 | 23.8 | 52 | 31.2 |
| 20 | 100 | 53 | 23.1 | 48 | 23.9 | 56 | 33.3 |
| 40 | 100 | 54 | 22.8 | 49 | 23.8 | 62 | 33.0 |
| 80 | 100 | 57 | 23.4 | 50 | 24.4 | 70 | 32.9 |
| 158 | 100 | 60 | 22.9 | 52 | 23.9 | 69 | 32.5 |
| 199 | 100 | 61 | 23.5 | 53 | 24.7 | 67 | 33.2 |
| 409 | 100 | 67 | 21.9 | 57 | 23.2 | 60 | 47.9 |
| 603 | 100 | 70 | 21.0 | 60 | 22.2 | 56 | 31.0 |
| 803 | 100 | 72 | 20.3 | 62 | 21.6 | 53 | 30.5 |
| 1303 | 100 | 74 | 20.2 | 65 | 21.4 | 48 | 30.3 |
| 1602 | 100 | 74 | 21.4 | 67 | 23.6 | 47 | 35.3 |
| 2001 | 100 | 74 | 20.3 | 73 | 23.8 | 40 | 39.5 |
| 2498 | 100 | 76 | 22.9 | 74 | 26.2 | 36 | 41.4 |

[a]Time since start of heating at 100°C

**Table A- II: Relative humidity (RH) and temperature (*T*) recorded by sensors while the heater *T* was set to 140°C in cell S/B (sensor 1 placed at 40 cm from the bottom, sensor 2 at 22 cm and sensor 3 at 10 cm)**

| Time[a] (h) | Time[b] (h) | RH1 (%) | T1 (°C) | RH2 (%) | T2 (°C) | RH3 (%) | T3 (°C) |
|---|---|---|---|---|---|---|---|
| 2499 | 1 | 76 | 23.0 | 74 | 26.3 | 36 | 41.5 |
| 2500 | 2 | 76 | 23.0 | 74 | 26.4 | 37 | 42.4 |
| 2503 | 5 | 76 | 23.1 | 74 | 26.6 | 41 | 46.5 |
| 2508 | 10 | 76 | 23.1 | 75 | 27.4 | 42 | 49.8 |
| 2518 | 20 | 76 | 23.6 | 76 | 28.6 | 42 | 51.5 |
| 2538 | 40 | 76 | 23.9 | 77 | 29.2 | 40 | 51.9 |
| 2580 | 82 | 76 | 24.2 | 78 | 29.3 | 37 | 51.9 |

| Time[a] (h) | Time[b] (h) | RH1 (%) | T1 (°C) | RH2 (%) | T2 (°C) | RH3 (%) | T3 (°C) |
|---|---|---|---|---|---|---|---|
| 2656 | 158 | 76 | 23.8 | 80 | 29.0 | 34 | 51.6 |
| 2700 | 202 | 76 | 22.7 | 80 | 28.0 | 33 | 50.8 |
| 2907 | 409 | 78 | 23.8 | 81 | 28.9 | 29 | 51.7 |
| 3103 | 605 | 78 | 22.0 | 80 | 27.1 | 27 | 50.4 |
| 3300 | 802 | 80 | 23.8 | 79 | 28.8 | 26 | 51.7 |
| 3692 | 1194 | 82 | 22.8 | 77 | 27.8 | 24 | 51.0 |

[a]Time since start of heating at 100°C; [b]Time since start of heating at 140°C

**Table A- III: Relative humidity (RH) and temperature (*T*) recorded by sensors while the heater *T* was set to 100°C in cell B (sensor 1 placed at 40 cm from the bottom, sensor 2 at 22 cm and sensor 3 at 10 cm)**

| Time[a] (h) | Heater *T* (°C) | RH1 (%) | T1 (°C) | RH2 (%) | T2 (°C) | RH3 (%) | T3 (°C) |
|---|---|---|---|---|---|---|---|
| 0 | 22 | 40 | 21.5 | | | 40 | 21.4 |
| 1 | 100 | 40 | 21.6 | | | 40 | 21.4 |
| 2 | 100 | 40 | 21.7 | | | 40 | 22.3 |
| 5 | 100 | 40 | 22.0 | | | 43 | 29.8 |
| 10 | 100 | 40 | 22.2 | | | 45 | 34.4 |
| 20 | 100 | 40 | 22.4 | | | 46 | 35.6 |
| 40 | 100 | 40 | 22.6 | 42 | 25.2 | 48 | 35.9 |
| 81 | 100 | 40 | 22.4 | 42 | 24.9 | 51 | 35.5 |
| 153 | 100 | 40 | 22.0 | 43 | 24.4 | 55 | 35.0 |
| 201 | 100 | 40 | 21.3 | 43 | 23.8 | 56 | 34.4 |
| 415 | 100 | 40 | 21.1 | 45 | 23.6 | 57 | 34.1 |
| 599 | 100 | 41 | 21.9 | 47 | 24.6 | 55 | 34.8 |
| 803 | 100 | 41 | 18.9 | 48 | 21.7 | 53 | 32.3 |
| 1003 | 100 | 41 | 20.1 | 49 | 22.7 | 52 | 33.1 |
| 1200 | 100 | 42 | 20.0 | 50 | 22.6 | 50 | 32.9 |
| 1402 | 100 | 42 | 20.8 | 51 | 23.2 | 48 | 33.5 |
| 1800 | 100 | 43 | 21.3 | 54 | 27.4 | 45 | 42.0 |
| 2333 | 100 | 45 | 23.9 | 56 | 29.9 | 40 | 43.9 |
| 2803 | 100 | 46 | 24.3 | 56 | 30.3 | 37 | 44.2 |
| 3300 | 100 | 47 | 22.9 | 55 | 28.9 | 35 | 43.1 |
| 3524 | 100 | 48 | 23.3 | 55 | 29.3 | 34 | 43.4 |

[a]Time since start of heating at 100°C

**Table A- IV: Relative humidity (RH) and temperature (*T*) recorded by sensors while the heater *T* was set to 140°C in cell B (sensor 1 placed at 40 cm from the bottom, sensor 2 at 22 cm and sensor 3 at 10 cm)**

| Time[a] (h) | Time[b] (h) | RH1 (%) | T1 (°C) | RH2 (%) | T2 (°C) | RH3 (%) | T3 (°C) |
|---|---|---|---|---|---|---|---|
| 3529 | 2 | 48 | 23.3 | 55 | 29.3 | 35 | 44.6 |
| 3533 | 5 | 48 | 23.6 | 55 | 30.2 | 37 | 49.9 |
| 3538 | 10 | 48 | 24.0 | 56 | 32.1 | 39 | 53.6 |
| 3548 | 20 | 48 | 24.6 | 56 | 33.8 | 40 | 55.4 |
| 3568 | 40 | 48 | 25.1 | 57 | 34.6 | 41 | 55.9 |
| 3607 | 79 | 48 | 25.3 | 57 | 34.7 | 40 | 56.0 |
| 3683 | 155 | 49 | 25.6 | 58 | 35.0 | 38 | 56.1 |
| 3731 | 203 | 49 | 25.8 | 59 | 35.1 | 37 | 56.2 |
| 3939 | 411 | 49 | 25.1 | 59 | 34.5 | 34 | 55.6 |
| 4131 | 603 | 50 | 27.5 | 60 | 36.7 | 32 | 57.3 |
| 4331 | 803 | 51 | 25.7 | 59 | 35.1 | 30 | 56.0 |
| 4531 | 1003 | 52 | 27.0 | 59 | 36.2 | 29 | 56.9 |
| 4851 | 1323 | 53 | 26.9 | 58 | 36.1 | 27 | 56.7 |
| 5015 | 1487 | 53 | 27.5 | 57 | 36.6 | 26 | 57.1 |

[a]Time since start of heating at 100°C; [b]Time since start of heating at 140°C